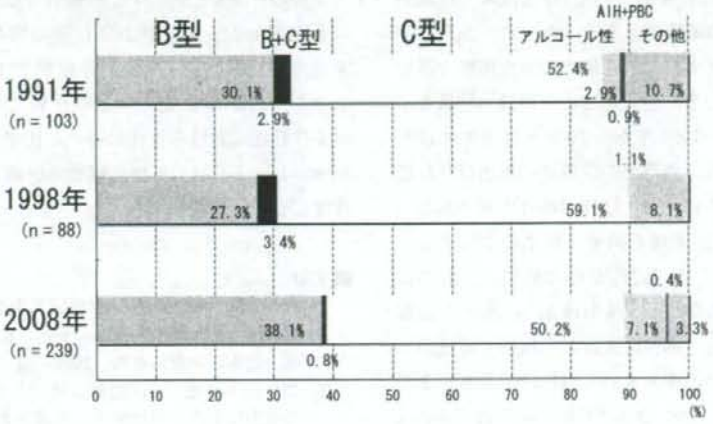

図2　肝がん合併肝硬変の成因 —頻度の経時的変化

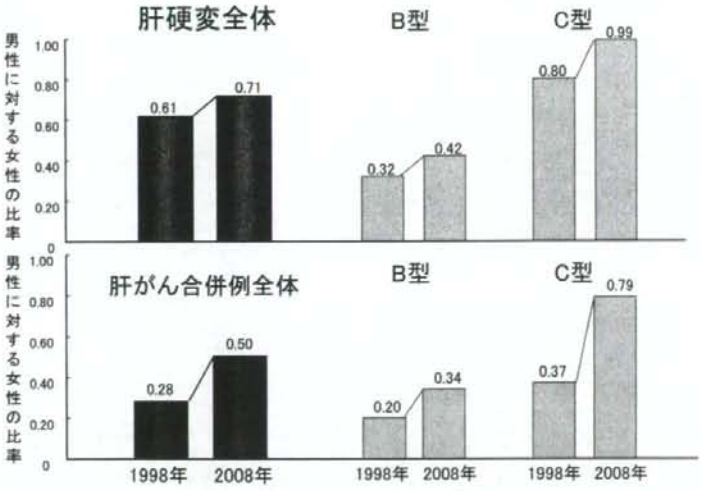

図3　肝硬変の性差 —女性比率の増加

し，B型では0.32から0.42へ，C型では0.80から0.99へと上昇を認めた．C型肝癌の発癌のリスクは男女間で差が見られなくなっていた．

考　察

全国の肝硬変患者の成因と比べて，従来より，北海道ではB型の比率が多い傾向を認めている．その理由のひとつに，北海道のHBs抗原陽性率が他の地域よりも高率であることが関連している可能性が考えられる．日本赤十字社の初回献血者（1995年から2000年まで）におけるHBs抗原陽性率を年代別にみると，16～19歳，20～29歳，30～39歳，40～49歳，50～59歳，60～75歳では，それぞれ0.23%，0.52%，0.84%，

1.19%，1.50%，1.27%であるが，北海道では，各年齢層で約3倍の陽性率を示している．肝硬変や肝癌などの好発年齢である50代以降では依然として3%台の陽性率である．さらに，当科へ紹介される肝癌患者には，他院での治療困難な高度進行肝癌症例が多く含まれている施設的特徴も一因と思われる．1997年から2008年3月までに当科に紹介された肝癌患者の肝硬変の原因は，B型が38%，C型が42%と，ほぼ同等の比率である．さらに，この10年間を前半と後半の5年ずつに分けて比較すると，B型/C型の頻度は，前半は31%/50%であったが，後半は41%/39%と逆転を示した．最近，高度に進行した状態で肝癌が発見され，集学的治療を求めて当科に紹介される例が増加しているが，医療機関で定期的にfollowされずに発癌する例には，B型関連患者が比較的多く含まれる可能性があり，このことも，当科の症例にB型が多いことの一因であると考えられた．

結　語

当科の肝硬変症例および肝癌合併症例の成因につき検討した．B型およびC型の関与は，肝硬変症例の80.3%，肝癌合併症例では88.1%であった．1998年調査時点との比較では，肝硬変および肝癌における女性の占める比率が上昇傾向を示した．とくに，C型肝硬変，肝癌において女性増加の傾向が著明であった．

■文献

1) 松嶋　喬，他：肝硬変の成因別実態．「肝硬変の成因別実態」太田康幸，原田　尚，小林健一編，日本医学館，東京，1992，p4-7.
2) 髭　修平，他：肝硬変の成因別実態．「肝硬変の成因別実態」小林健一，清澤研道，岡上　武編，中外医学社，東京，1999，p75-79.

Ⅱ エイズ (acquired immunodeficiency syndrome ; AIDS)

1. AIDS とはどういう病気か

●原因ウイルスと病態

AIDS とは HIV 感染症である.

Human Immunodeficiency Virus (HIV：ヒト免疫不全ウイルス) 感染症で Acquired Immuno Deficiency Syndrome (後天性免疫不全症候群) の略. わが国の感染者数は年間千人を超え, 感染爆発が懸念される.

HIV は, レトロウイルスであるため一度感染すると終生感染者となる. また免疫細胞, 特に CD4 陽性細胞に親和性が強い. HIV 感染後は急性期症状, 無症候性キャリアー, AIDS 関連症候群を経て, AIDS に至る.

8～9 割の感染者は感染後 10～15 年後に AIDS を発症する. ときに急激に AIDS を発症したり, 長期間免疫不全の徴候を示さなかったりする感染者も存在する. 発症した AIDS 患者は細胞性免疫不全の徴候を示し, 日和見感染症がみられる. それらの合併症に対する予防・治療法は進歩した. しかし, 中枢神経症状や悪性リンパ腫を伴うと予後はきわめて悪い. 感染者体内のウイルスはさまざまに変異し, 抗 HIV 免疫応答が有効に機能せず, 感染は持続する. 感染初期はマクロファージ好性のウイルス (R 5) が主で, 後に T 細胞好性 (X 4) のウイルスが出現する. 両者は異なった補受容体を使って感染する.

メモ HIV：レトロウイルスなのでウイルスの遺伝情報は RNA である. 感染細胞に侵入した後に, 逆転写酵素により RNA を DNA に変換する. レトロウイルスは腫瘍ウイルス, レンチウイルス, スプマウイルスなどがあるが, HIV はレンチウイルス. タイプⅠとタイプⅡが存在する.

タイプⅠは全世界に拡がっていて, 感染者数は 4,000 万人以上である. タイプⅡはアフリカ西海岸に散見されるが, 感染力, 発病性ともに低い. 感染者体内のウイルスは R5 と X4 に分類される. 標的細胞のウイルス受容体は CD4 分子と補受容体の 2 種類である. R5 と X4 は使用する補受容体 (ケモカイン受容体) が異なっている. R5 は

表 4　AIDS 指標症状

真菌感染症	原虫症	細菌感染症	ウイルス感染症	腫瘍	その他
カンジダ症 クリプトコッカス症 コクシジオイデス症 ヒストプラズマ症 ニューモシスチス肺炎	トキソプラズマ症 クリプトスポリジウム症 イソスポラ症	化膿性細菌感染症 サルモネラ菌血症 活動性結核 非定型抗酸菌症	サイトメガロウイルス感染症 単純ヘルペスウイルス感染症 進行性多巣性白質脳症	カポジ肉腫 原発性脳リンパ腫 非ホジキンリンパ腫 浸潤性子宮頸癌	反復性肺炎 リンパ性間質性肺炎 HIV 脳症 HIV 消耗性症候群

表 5　成人の HIV 感染者の診断基準（1993 年改訂版）

	臨床カテゴリー		
CD4 細胞数（/μl）	A 無症候性・急性期*2	B 症状あり	C AIDS 指標症状あり*3
500 以上	A1	B1	C1
200～499	A2	B2	C2
200 未満*1	A3	B3	C3

*1　A3，B3，C1～3 は拡大 AIDS 症例
*2　進行性全身性リンパ節腫大を含む
*3　AIDS 指標症状は表 4

CCR5 を，X4 は CXCR4 を使用するが，すでに 10 種のケモカイン受容体が補受容体の機能を有することが知られている．

メモ 日和見感染症：免疫機能が正常の個体には病原性をもたない病原体が免疫不全（特に T 細胞の機能低下）を招来した際に，さまざまな感染症を生ずる．老人や乳幼児，抗癌薬治療後，原発性免疫不全症候群患者も罹患しやすい．具体的な疾患名は表 4 に示した．また免疫不全に伴いやすい，カポジ肉腫，悪性リンパ腫なども含め，日和見疾患とも呼ぶ．

2．どのように考えて診断をつけていくか

診断のキーポイント
1．感染者は徐々に増加していて，一般開業医でもリスクファクターのない感染者に遭遇する
2．代表的なリスクファクターは，男子同性愛，麻薬中毒，血液製剤投与・輸血歴，海外渡航
3．発熱，下痢，リンパ節腫大があり，日和見感染や中枢神経症状を伴う
4．CD4 細胞減少，抗 HIV 抗体陽性

感染原因となる行為，たとえば，多数のパートナーとの性行為（わが国では男子同性愛行為での感染によるものが多い），注射針共有や輸血，臓器移植，血液製剤投与などが患者の背景に存在する．しかし初診者では背景がはっきりしない例も多い．感染後 3～6 週に発熱，感冒様症状，皮膚発疹，リンパ節腫脹，髄膜炎症状などの急性期症状を呈する．8 週までにほぼ全員に抗体が検出されるが，特殊な例では 1 年近く抗体が陽性化しない例もある．抗体検査を施行する際には，患者の同意をとる必要がある．また抗体陽性者を発見した際は，無症候であろうとも，保健所長を通して知事に報告する義務がある．ウイルス分離やウイルス抗原の検出によっても感染者を同定できる．感染者のウイルスの量が病勢の把握の，CD4 細胞数が疾患のステージ決定の最も良い指標となる．症状と CD4 細胞数を組み合わせた診断基準を紹介する（表 5）．CD4 細胞数が 200/μl 未満となったら症状のあるなしによらず AIDS と診断する．また CD4 細胞数によらず感染者が表 4 の疾患を併発したら AIDS と診断する．

3．主な治療法と日常生活管理の実際

治療のキーポイント
1．血漿中の HIV-RNA と CD4 細胞数を測定して病態を把握する
2．臨床症状，HIV-RNA の増加，CD4 細胞数の減少のいずれかがあれば抗ウイルス薬を投与する
3．CD4 細胞数が減少していれば，日和見感染症の予防・治療を開始する

a．ウイルス量と予後

HIV 感染症においては，推定で 100 億個の粒子が毎日産生され，ウイルスの半減期は 6 時間ときわめて短い．CD4 細胞も短い半減期で回転しているともいわれ，無症候時期でもダイナミックなウイルスと免疫の動態が存在する．血漿 HIV-RNA 量は発症の危険性を予知するのにきわめてよいマーカーとなりうるが最近ではウイルス量に関係ない免疫活生化が重要という説もある．

メモ 血漿 HIV-RNA 量：定量性 PCR の導入により HIV の RNA の定量がきわめて容易になった．治療開始時期，効果判定にはきわめて有用で，化学療法において，検出感度以下までに低下する例もある．また，HIV の量が 500/μl 以下だと 10 年後の AIDS 発症率はきわめて低いといわれていたが，HIV-RNA 量と CD4 数の減少に相関が

ないとするデータもある.

b. HAARTとその問題点

HAARTによりウイルス量の低下とCD4細胞数の増加をはかる.

逆転写酵素阻害薬とプロテアーゼ阻害薬を組み合わせるhighly active anti-retroviral therapy (HAART)によりAIDSの進行を回避できる. 治療開始時期, 副作用など抱える問題は多々ある. ウイルスが体内から消失するわけではなく, リンパ節や末梢血CD4細胞中では治療中にもかかわらず, 複製がみられ, 感染者であることにはかわりはない.

メモ プロテアーゼ阻害薬：プロテアーゼはHIV自身が有する自己の蛋白の成熟を司る蛋白分解酵素である. アスパルティックプロテアーゼの1種. さまざまな阻害薬が感染者の治療に考案されまた使用されている.

c. 日和見感染症に対する予防・治療

カンジダ症は免疫機能が保たれている時期でも口腔内に生じやすいが, フルコナゾールなどの抗真菌薬により重症化を阻止できる. CD4細胞数が200/μl未満ではさまざまな日和見疾患が生ずる. この時期の患者では, ニューモシスチス肺炎は致命率, 発症率ともに高いので, ST合剤による予防を開始し, サイトメガロウイルス感染は網膜に高頻度で発症するので, 定期的な検査が必要である. また結核の合併はCD4数に関係なく生ずる. 感染が危惧される際はINHの予防投与を行うが, BCG接種は禁忌である. 日和見感染症を合併している場合は, 免疫再構築症候群を避けるため, 日和見感染症の治療を優先する.

メモ 免疫再構築症候群：HAARTにより免疫機能が回復する過程で, 治癒していたあるいは隠れていた日和見感染が増悪し, 新たな日和見感染症が出現する場合があり, これを免疫再構築症候群 (IRIS) と呼んでいる.

d. 感染予防

感染者由来の体液で, 感染源となりうるものは感染性のウイルスを一定量以上含むものである. これらの体液においては特に感染予防に注意しなければならない. 注意を払う体液を表6に示す. 血液を含む場合にはどのような体液でも感染予防に注意を払わなければならない. なぜならば血液は遊離ウイルス以外にきわめて感染力の強い, 白血球を含むからである. 細胞と細胞による感染はきわめて効率的なので, 皮膚に傷や湿疹を有する場合には適宜防護して診療・看護にあたる必要がある. 性病の存在は感染を助長する. 無防備な性行為を避けると同時に, コンドームの使用が感染予防には効果的である.

表6　体液に対する一般的注意 (HIV感染症)

注意の必要な体液	肉眼的な血液がみえなければ注意が不要な体液
血液	糞
精液	鼻汁
膣分泌液	痰
羊水	汗
脳脊髄液	涙
心嚢液	尿
腹水	嘔吐物
胸水	
滑膜液	
母乳	
唾液*	

*歯科に限る. 歯科の扱う唾液はほとんど血液を含んでいる.

e. 日常生活管理

免疫機能の維持が大事であるが, むやみな免疫賦活はウイルスの産生を高めるので, 注意を要する. かぜ, ストレスを避けることが望ましい. CD4細胞数が500/μl未満では日和見感染が生じやすくなり, 十分な栄養の補給と適切な休養が望ましい. また全病期を通じてカウンセリングを必要とする. また無症候時期でも治療中でも体液にはウイルス感染細胞が存在するので, 感染の拡大を防ぐ指導が必要である.

(服部俊夫)

PPARα activation is essential for HCV core protein–induced hepatic steatosis and hepatocellular carcinoma in mice

Naoki Tanaka,[1,2] Kyoji Moriya,[3] Kendo Kiyosawa,[2] Kazuhiko Koike,[3] Frank J. Gonzalez,[4] and Toshifumi Aoyama[1]

[1]Department of Metabolic Regulation, Institute on Aging and Adaptation, Shinshu University Graduate School of Medicine, Matsumoto, Nagano, Japan.
[2]Division of Gastroenterology, Department of Internal Medicine, Shinshu University School of Medicine, Matsumoto, Nagano, Japan.
[3]Department of Infectious Diseases, Internal Medicine, Graduate School of Medicine, University of Tokyo, Tokyo, Japan.
[4]Laboratory of Metabolism, National Cancer Institute, NIH, Bethesda, Maryland, USA.

Transgenic mice expressing HCV core protein develop hepatic steatosis and hepatocellular carcinoma (HCC), but the mechanism underlying this process remains unclear. Because PPARα is a central regulator of triglyceride homeostasis and mediates hepatocarcinogenesis in rodents, we determined whether PPARα contributes to HCV core protein–induced diseases. We generated PPARα-homozygous, -heterozygous, and -null mice with liver-specific transgenic expression of the core protein gene (*Ppara*$^{+/+}$:HCVcpTg, *Ppara*$^{+/-}$:HCVcpTg, and *Ppara*$^{-/-}$:HCVcpTg mice. Severe steatosis was unexpectedly observed only in *Ppara*$^{+/+}$:HCVcpTg mice, which resulted from enhanced fatty acid uptake and decreased mitochondrial β-oxidation due to breakdown of mitochondrial outer membranes. Interestingly, HCC developed in approximately 35% of 24-month-old *Ppara*$^{+/+}$:HCVcpTg mice, but tumors were not observed in the other genotypes. These phenomena were found to be closely associated with sustained PPARα activation. In *Ppara*$^{+/-}$:HCVcpTg mice, PPARα activation and the related changes did not occur despite the presence of a functional *Ppara* allele. However, long-term treatment of these mice with clofibrate, a PPARα activator, induced HCC with mitochondrial abnormalities and hepatic steatosis. Thus, our results indicate that persistent activation of PPARα is essential for the pathogenesis of hepatic steatosis and HCC induced by HCV infection.

Introduction

HCV is one of the major causes of chronic hepatitis, whereas patients with persistent HCV infection have a high incidence of hepatocellular carcinoma (HCC) (1, 2). Occurrence of HCC associated with chronic HCV infection has increased over the past 2 decades (3–5), and chronic HCV infection is recognized as a serious debilitating disease. However, the mechanism in which chronic HCV infection mediates hepatocarcinogenesis remains unclear.

HCV core protein was shown to have oncogenic potential (6). To examine how HCV core protein participates in HCV-related hepatocarcinogenesis, transgenic mouse lines were established in which HCV core protein is expressed constitutively in liver at cellular levels similar to those found in chronic HCV-infected patients (7). These mice exhibited hepatic steatosis (7) and insulin resistance (8) as early as 3 months of age; on further aging, these symptoms worsened and hepatic adenomas developed in approximately 30% of mice between 16 and 18 months of age (9). Finally, HCC was found within hepatic adenomas in a classic "nodule-in-nodule" pathology (9). Interestingly, no hepatic inflammation or fibrosis was found in these mice throughout the course of HCC development (9), which suggested that the HCV core protein itself induces hepatic steatosis and HCC independently of hepatitis.

Several studies support the contention that hepatic steatosis promotes the development of HCC (10). Epidemiologic data have identified hepatic steatosis as a major accelerating factor of hepatocarcinogenesis in chronic HCV-infected patients (11). Moreover, increases in ROS production that can cause oxidative DNA damage, mitochondrial abnormalities, and accelerated hepatocyte proliferation were observed in the steatotic livers (12–14). Thus, an intriguing possibility has emerged that alteration of fatty acid metabolism in hepatocytes may be central to the pathogenesis of HCC induced by HCV core protein.

PPARs are ligand-activated nuclear receptors belonging to the steroid/thyroid hormone receptor superfamily; 3 isoforms designated as α, β/δ, and γ exist, all of which are involved in lipid homeostasis (15). PPARα regulates constitutive transcription of genes encoding fatty acid–metabolizing enzymes (16) and is associated with the maintenance of fatty acid transport and metabolism, primarily in liver, kidney, and heart. Administration of PPARα agonists, such as the widely prescribed fibrate drugs clofibrate, gemfibrozil, and fenofibrate, ameliorate hyperlipidemia in humans (17) and hepatic steatosis in mice (18).

On the other hand, long-term administration of PPARα ligands to rodents causes accelerated hepatocyte proliferation, increased ROS generation, and development of HCC (19, 20). Disruption of the PPARα gene was shown to prevent the development of HCC caused by long-term exposure to PPARα activators (21). Interestingly, accumulation of fatty acids/triglycerides in hepatocytes

Nonstandard abbreviations used: ACC, acetyl-CoA carboxylase; AOX, acyl-CoA oxidase; CDK, cyclin-dependent kinase; CYP4A1, cytochrome P450 4A1; FAS, fatty acid synthase; FAT, fatty acid translocase; FATP, fatty acid transport protein; HCC, hepatocellular carcinoma; HCVcpTg, HCV core protein–expressing transgenic; L-FABP, liver fatty acid-binding protein; MCAD, medium-chain acyl-CoA dehydrogenase; MTP, microsomal transfer protein; 8-OHdG, 8-hydroxy-2′-deoxyguanosine; PCNA, proliferating cell nuclear antigen; RXRα, retinoid X receptor α.

Conflict of interest: The authors have declared that no conflict of interest exists.
Citation for this article: *J. Clin. Invest.* **118**:683–694 (2008). doi:10.1172/JCI33594.

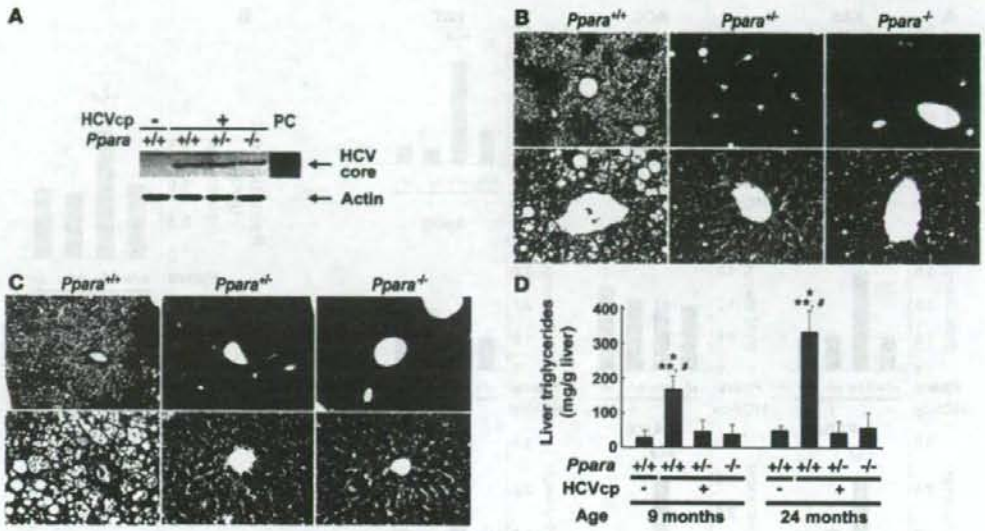

Figure 1

Phenotype changes in transgenic mouse liver. (**A**) Immunoblot analysis of HCV core protein expression in livers of 9-month-old mice. Because no significant individual differences in the same mouse group were found in the preliminary experiments, 10 mg of liver prepared from each mouse (n = 6 /group) was mixed and homogenized. Whole-liver lysate (50 μg protein) was loaded in each well. The band of actin was used as the loading control. Results are representative of 4 independent experiments. PC, lysate prepared from COS-1 cells overexpressing HCV core protein as a positive control. (**B**) Histological appearance of hematoxylin- and eosin-stained liver sections from 9-month-old HCVcpTg mice. Upper and lower rows show a lower (×40) and higher (×400) magnification, respectively. Microvesicular and macrovesicular steatosis was found only in *Ppara*$^{+/+}$:HCVcpTg mice. No inflammation or hepatocyte degeneration was evident in any of the genotypes. (**C**) Histological appearance of hematoxylin- and eosin-stained liver sections from 24-month-old HCVcpTg mice. Upper and lower rows show a lower (×40) and higher (×400) magnification, respectively. Hepatic steatosis was marked in *Ppara*$^{+/+}$:HCVcpTg mice, but not in other mice. Hepatic inflammation, fibrosis, and hepatocyte degeneration were not observed. In *Ppara*$^{+/-}$:HCVcpTg and *Ppara*$^{-/-}$:HCVcpTg mice, dysplastic hepatocytes and precancerous lesions were not detected throughout the entire liver. (**D**) Content of liver triglycerides. Results are expressed as the mean ± SD (n = 6/group) and compared between genotypes at the same age. *P < 0.05 compared with *Ppara*$^{+/+}$ nontransgenic mice; **P < 0.05 compared with *Ppara*$^{+/-}$:HCVcpTg mice; #P < 0.05 compared with *Ppara*$^{-/-}$:HCVcpTg mice.

could lead to continuous PPARα activation because of the presence of fatty acid metabolites that serve as natural PPARα ligands. For example, mice lacking expression of the peroxisomal acyl-CoA oxidase (AOX) gene showed massive accumulation of very-long-chain fatty acids in hepatocytes, severe microvesicular steatosis, chronic PPARα activation, and development of hepatic adenoma and HCC by 15 months of age (22). These results suggest a strong contribution of activated PPARα to liver tumorigenesis.

On the basis of several lines of evidence, we hypothesized that PPARα might contribute to hepatocarcinogenesis in HCV core protein–expressing transgenic (HCVcpTg) mice. To explore this possibility, PPARα-homozygous (*Ppara*$^{+/+}$), PPARα-heterozygous (*Ppara*$^{+/-}$), and PPARα-null (*Ppara*$^{-/-}$) mice bearing the HCV core protein gene, designated *Ppara*$^{+/+}$:HCVcpTg, *Ppara*$^{+/-}$:HCVcpTg, and *Ppara*$^{-/-}$:HCVcpTg mice, were generated, and phenotypic changes were examined. Surprisingly, we found that severe hepatic steatosis and HCC induced by HCV core protein developed only in *Ppara*$^{+/+}$ mice, which were related to persistent PPARα activation.

Results

Expression of HCV core protein in transgenic mice. *Ppara*$^{-/-}$:HCVcpTg and *Ppara*$^{+/-}$:HCVcpTg mice appeared healthy, and body weight in both genotypes was similar to that of *Ppara*$^{+/+}$:HCVcpTg and *Ppara*$^{+/+}$ mice without the transgene. When hepatic expression of HCV core protein in 9-month-old transgenic mice was examined by immunoblot analysis, it was similar among *Ppara*$^{+/+}$:HCVcpTg, *Ppara*$^{+/-}$:HCVcpTg, and *Ppara*$^{-/-}$:HCVcpTg mice (Figure 1A) and was also similar to expression in HCVcpTg mice reported previously (7, 9). Age and sex had only a minor influence on the hepatic expression of HCV core protein.

Requirement of homozygous PPARα for the development of hepatic steatosis in transgenic mice. Livers of 9-month-old male HCVcpTg mice with or without the *Ppara* allele were examined. Those of *Ppara*$^{+/+}$:HCVcpTg mice were soft, slightly enlarged, and light in color and histologically showed macrovesicular and microvesicular steatosis with no apparent inflammation or hepatocyte necrosis (Figure 1B), in agreement with previous reports (7, 9). Biochemical analysis of liver extracts showed marked hepatic accumulation of triglycerides (Figure 1D). In contrast, livers of 9-month-old *Ppara*$^{+/-}$:HCVcpTg and *Ppara*$^{-/-}$:HCVcpTg mice showed neither histological abnormalities nor accumulation of triglycerides (Figure 1, B and D). Hepatic levels of free fatty acids in *Ppara*$^{+/+}$:HCVcpTg mice were approximately 3 times those in *Ppara*$^{+/-}$:HCVcpTg and *Ppara*$^{-/-}$:HCVcpTg mice or *Ppara*$^{+/+}$ mice not expressing the HCV core protein.

In 24-month-old *Ppara*$^{+/+}$:HCVcpTg mice, hepatic steatosis was found (Figure 1C), and the hepatic levels of triglycerides were further increased (Figure 1D). Apparent inflammation, hepatocyte

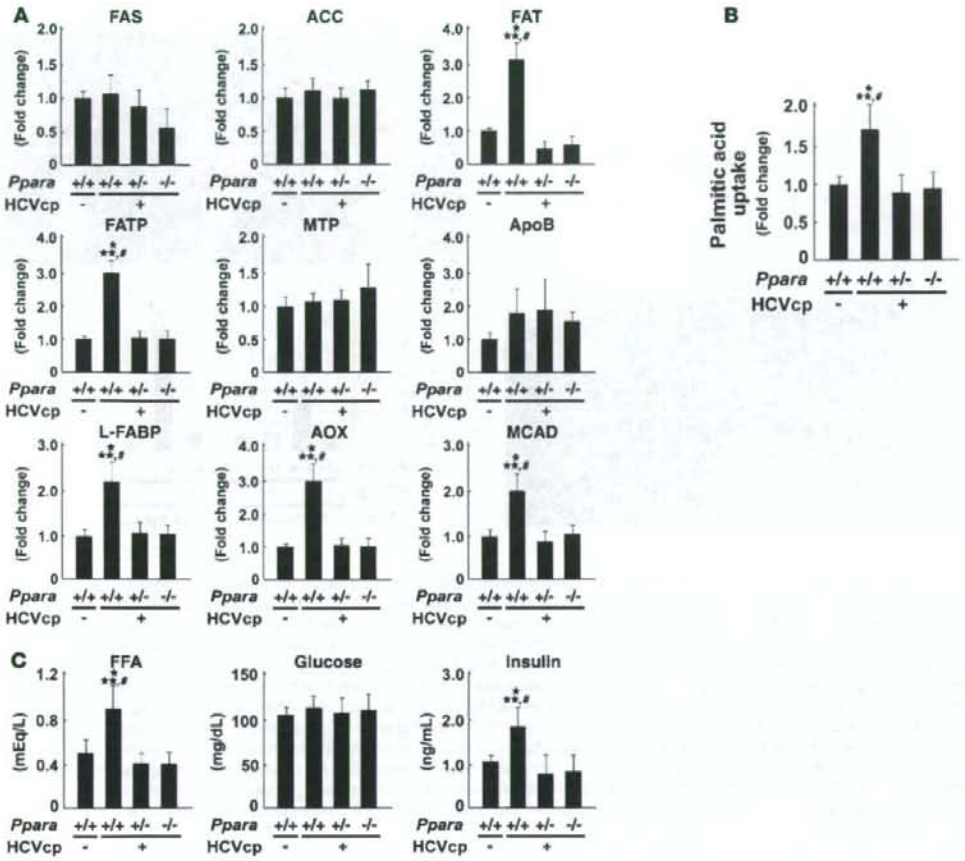

Figure 2

Analyses of factors associated with hepatic fatty acid and triglyceride metabolism. (**A**) Expression of genes associated with fatty acid and triglyceride metabolism in 9-month-old mouse livers. Total RNA was extracted from each mouse liver, and mRNA levels were determined by RT-PCR. mRNA levels were normalized by those of GAPDH and subsequently normalized by those in *Ppara*$^{+/+}$ nontransgenic mice. Results are expressed as the mean ± SD (n = 6/group). *P < 0.05 compared with *Ppara*$^{+/+}$ nontransgenic mice; **P < 0.05 compared with *Ppara*$^{+/-}$:HCVcpTg mice; #P < 0.05 compared with *Ppara*$^{-/-}$:HCVcpTg mice. (**B**) Uptake of fatty acids in 9-month-old mouse livers. Liver slices obtained from 3 mice in each group were incubated in medium containing 0.8 mM [1-^{14}C]palmitic acid for 7 h. Fatty acid uptake ability was estimated by the sum of palmitic acid converted to CO_2 and ketone bodies with that incorporated into total cellular lipids after incubation. The experiment was repeated 3 times. Results were normalized by those of *Ppara*$^{+/+}$ nontransgenic mice and expressed as the mean ± SD. (**C**) Plasma concentrations of free fatty acids, glucose, and insulin. After an overnight fast, blood was obtained from each mouse and the above variables were determined. Results are expressed as the mean ± SD (n = 6/group).

degeneration and necrosis, and fibrosis were not detected. On the other hand, *Ppara*$^{+/-}$:HCVcpTg and *Ppara*$^{-/-}$:HCVcpTg mice showed no steatosis (Figure 1, C and D). These results indicate that hepatic steatosis develops in *Ppara*$^{+/+}$:HCVcpTg mice, but not in *Ppara*$^{+/-}$:HCVcpTg and *Ppara*$^{-/-}$:HCVcpTg mice.

Hepatic fatty acid and triglyceride metabolism in transgenic mice. To investigate the mechanism responsible for the development of severe steatosis in *Ppara*$^{+/+}$:HCVcpTg mice, the expression of genes associated with fatty acid and triglyceride metabolism in the livers of 9-month-old mice was analyzed using the quantitative RT-PCR method. As shown in Figure 2A, the mRNA levels of genes related to de novo lipogenesis (fatty acid synthase [FAS] and acetyl-CoA carboxylase [ACC]) and secretion of VLDL (microsomal transfer protein [MTP] and apoB) were constant in all groups. The mRNA levels of fatty acid translocase (FAT) and fatty acid transport protein (FATP), which are associated with the uptake of fatty acids into hepatocytes, were significantly increased only in *Ppara*$^{+/+}$:HCVcpTg mice, but the mRNA levels of hepatic triglyceride lipase, another contributor to fatty acid uptake, remained unchanged (data not shown). The mRNA levels of liver fatty acid binding protein (L-FABP) were also elevated only in *Ppara*$^{+/+}$:HCVcpTg mice. Surprisingly, the mRNA levels of AOX and medium-chain acyl-CoA

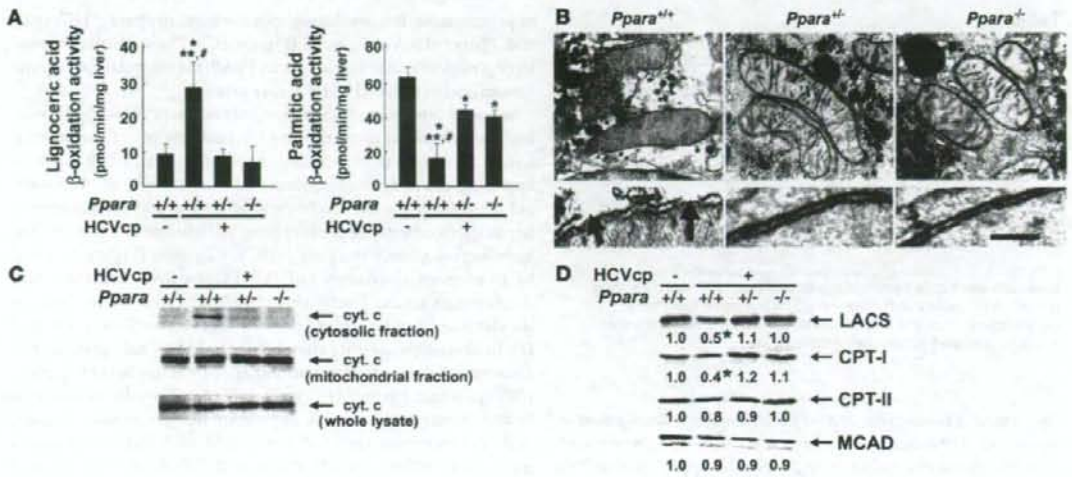

Figure 3

Analyses of mitochondrial abnormalities. (**A**) Lignoceric and palmitic acid β-oxidation activities in 9-month-old mice. Results are expressed as the mean ± SD (n = 6/group). *P < 0.05 compared with *Ppara*$^{+/+}$ nontransgenic mice; **P < 0.05 compared with *Ppara*$^{+/-}$:HCVcpTg mice; #P < 0.05 compared with *Ppara*$^{-/-}$:HCVcpTg mice. (**B**) Electron microscopic features of hepatic mitochondria of 9-month-old HCVcpTg mice. Upper and lower rows show a lower and higher magnification, respectively. In *Ppara*$^{+/+}$:HCVcpTg mice, some mitochondria showing discontinuance of outer membranes (arrows) and amorphous inner structures were observed. In *Ppara*$^{+/-}$:HCVcpTg and *Ppara*$^{-/-}$:HCVcpTg mice, mitochondria appeared normal; the scale bars represent 200 nm (top) and 30 nm (bottom), respectively. (**C**) Immunoblot analysis of cytochrome *c* in 9-month-old mice. Whole-liver lysate, mitochondrial fraction, or cytosolic fraction (50 μg protein) was loaded in each well. Results are representative of 4 independent experiments. (**D**) Immunoblot analysis of representative mitochondrial β-oxidation enzymes using a mitochondrial fraction prepared from 9-month-old mouse livers. The mitochondrial fraction (20 μg protein) was loaded in each well. Results are representative of 4 independent experiments. The band intensity was quantified densitometrically and normalized by that in *Ppara*$^{+/+}$ nontransgenic mouse. The mean value of the fold changes is shown under the representative band. LACS, long-chain acyl-CoA synthase; CPT, carnitine palmitoyl-CoA transferase.

dehydrogenase (MCAD), a rate-limiting enzymes in the peroxisomal and mitochondrial β-oxidation pathways, respectively, were significantly increased in *Ppara*$^{+/+}$:HCVcpTg mice. When fatty acid uptake ability was measured in fresh liver slices, it was significantly enhanced only in *Ppara*$^{+/+}$:HCVcpTg mice (Figure 2B). Additionally, plasma free fatty acid levels were higher in these mice than in mice in the other groups. Although there were no differences in fasting plasma glucose levels between the groups, hyperinsulinemia was observed only in *Ppara*$^{+/+}$:HCVcpTg mice (Figure 2C), in agreement with the previous observation that significant insulin resistance developed in these mice (8). Similar results were obtained from 24-month-old mice (data not shown). These results combined show that the increased plasma fatty acid levels, which were likely due to enhanced peripheral fatty acid release caused by insulin resistance, and the increase in fatty acid uptake ability are consistent with steatogenesis in *Ppara*$^{+/+}$:HCVcpTg mice.

Decreased mitochondrial β-oxidation in transgenic mice. Although the transcriptional activities of major β-oxidation enzymes were markedly increased, *Ppara*$^{+/+}$:HCVcpTg mice had severe steatosis. To explore this discrepant result, peroxisomal and mitochondrial β-oxidation activities were measured using lignoceric and palmitic acids as substrates, respectively. The lignoceric acid–degrading capacity was increased only in *Ppara*$^{+/+}$:HCVcpTg mice, where it corresponded to an increase in AOX expression. However, the capacity for palmitic acid degradation, which occurs particularly in mitochondria, was significantly lower in *Ppara*$^{+/+}$:HCVcpTg mice than in *Ppara*$^{+/-}$:HCVcpTg and *Ppara*$^{-/-}$:HCVcpTg mice (Figure 3A). Thus, decreased mitochondrial β-oxidation ability was considered to be another important mechanism for the development of steatosis induced by the core protein.

We further evaluated mitochondrial abnormalities. In electron microscopic examination, discontinuous outer membranes (Figure 3B, arrows) and lack of an internal structure were observed in some mitochondria of *Ppara*$^{+/+}$:HCVcpTg mouse livers, in agreement with the previous report (9). However, these abnormalities were not seen in *Ppara*$^{+/-}$:HCVcpTg and *Ppara*$^{-/-}$:HCVcpTg mice (Figure 3B). Immunoblot analysis showed that cytochrome *c*, which is usually localized in the mitochondrial intermembrane space, was present in the cytosolic fractions of *Ppara*$^{+/+}$:HCVcpTg mice (Figure 3C). Moreover, immunoblot analysis using mitochondrial fractions showed that the expression levels of long-chain acyl-CoA synthase and carnitine palmitoyl-CoA transferase-I, which are enzymes indispensable to the initial step of mitochondrial β-oxidation and are localized mainly in mitochondrial outer membranes, were significantly decreased only in *Ppara*$^{+/+}$:HCVcpTg mice (Figure 3D).

Overall, these results suggest that homozygous PPARα is essential to the pathogenesis of hepatic steatosis induced by the HCV core protein, which results from a decrease in mitochondrial fatty acid degradation capacity caused by the breakdown of mitochondrial outer membranes and a disproportionate increase in the uptake of fatty acids. Interestingly, steatosis and the related changes did not occur in *Ppara*$^{+/-}$ and *Ppara*$^{-/-}$ mice expressing the HCV core protein, which suggested that these changes were not caused by the core protein itself.

Table 1
Incidence of HCC in 24-month-old mice

HCV core protein	*Ppara*	Mice (*n*)	Mice with HCC (*n*)	Incidence (%)
–	+/+	20	0	0
–	+/–	18	0	0
–	–/–	20	0	0
+	+/+	17	6	35.3[A]
+	+/–	16	0	0
+	–/–	14	0	0

Mice were killed at 24 months of age for analysis. HCC was diagnosed according to histological findings. [A]$P < 0.05$ compared with *Ppara*$^{+/+}$ nontransgenic mice, $P < 0.05$ compared with *Ppara*$^{+/-}$:HCVcpTg mice, $P < 0.05$ compared with *Ppara*$^{-/-}$:HCVcpTg mice.

Requirement of homozygous PPARα for hepatic tumor development in transgenic mice. At 9 months of age, hepatic nodules were not observed at all in transgenic mice, whereas, at 24 months, approximately 35% of *Ppara*$^{+/+}$:HCVcpTg mice had macroscopically evident hepatic nodules (Table 1). Microscopically, these nodules had the appearance of well-differentiated HCC with trabecular features, which was consistent with the previous report (9). Surprisingly, *Ppara*$^{+/-}$:HCVcpTg and *Ppara*$^{-/-}$:HCVcpTg mice of the same ages developed no evidence of hepatic tumors, despite the expression of HCV core protein at similar levels to those found in *Ppara*$^{+/+}$:HCVcpTg mice (Table 1). Microscopic examination showed that there were no dysplastic cells or precancerous lesions throughout the livers in *Ppara*$^{+/-}$:HCVcpTg and *Ppara*$^{-/-}$:HCVcpTg mice (Figure 1C). These results provide strong evidence that homozygous PPARα is essential for hepatic tumorigenesis induced by HCV core protein.

Increased hepatocyte proliferation only in Ppara$^{+/+}$*:HCVcpTg mice.* Because sustained acceleration of hepatocyte proliferation relative to apoptosis may promote the development of HCC, these opposing processes were quantified in the livers of 24-month-old mice. Both the liver-to-body weight ratio and the number of hepatocytes expressing proliferating cell nuclear antigen (PCNA) were increased only in *Ppara*$^{+/+}$:HCVcpTg mice (Figure 4, A and B). In contrast, the number of TUNEL-positive hepatocytes and the hepatic caspase 3 activity, indicators of hepatocyte apoptosis, remained similar among the 3 mouse strains (Figure 4, C and D). Interestingly, despite the presence of HCV core protein, the amounts of these proliferative and apoptotic markers in *Ppara*$^{+/-}$:HCVcpTg and *Ppara*$^{-/-}$:HCVcpTg mice were similar to those in *Ppara*$^{+/+}$ nontransgenic mice. Expression levels of several proteins, such as protooncogenes (c-Fos and c-Myc), cell-cycle regulators (cyclin D1, cyclin-dependent kinase [CDK] 4, and PCNA), and phosphorylated ERK 1 and 2, all of which are associated with hepatocyte proliferation, were elevated in *Ppara*$^{+/+}$:HCVcpTg mice but not in other genotypes (Figure 4, E and F).

Increased oxidative stress and DNA damage only in Ppara$^{+/+}$*:HCVcpTg mice.* HCV core protein is associated with increased production of ROS (23). Enhanced ROS production induces nuclear DNA damage, which results in the initiation of hepatocarcinogenesis, and can also injure organelles, which can result in disorders in their

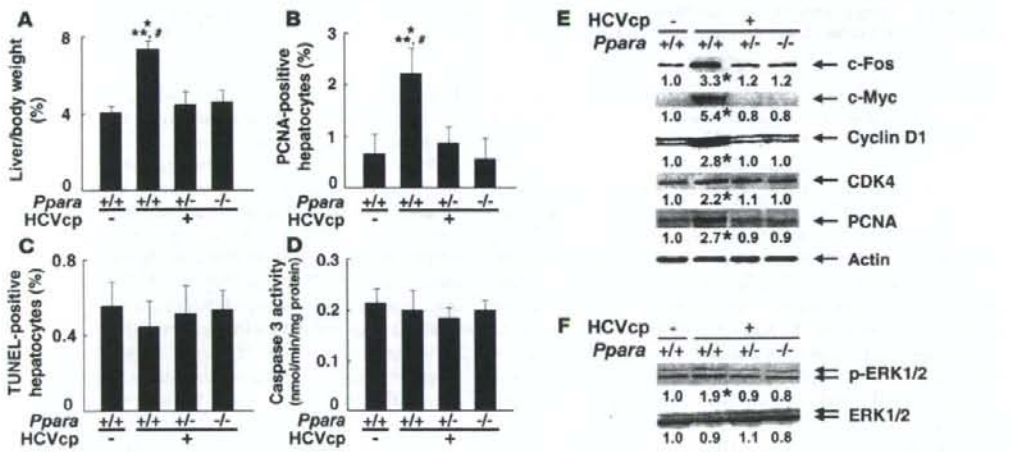

Figure 4
Increased hepatocyte proliferation in *Ppara*$^{+/+}$:HCVcpTg mice at 24 months of age. (**A**) Liver-to-body-weight ratio. Results are expressed as the mean ± SD (n = 6/group). (**B**) Numbers of proliferating hepatocytes. Two thousand hepatocytes were examined in each mouse, and hepatocyte nuclei positive for anti-PCNA antibody were counted. Results are expressed as the mean ± SD (n = 6/group). For **A** and **B**, comparisons are designated as follows: *$P < 0.05$ compared with *Ppara*$^{+/+}$ nontransgenic mice; **$P < 0.05$ compared with *Ppara*$^{+/-}$:HCVcpTg mice; #$P < 0.05$ compared with *Ppara*$^{-/-}$:HCVcpTg mice. (**C**) Numbers of apoptotic hepatocytes. Liver sections were subjected to TUNEL staining, and TUNEL-positive hepatocyte nuclei were counted in 2,000 hepatocytes from each mouse. Results are expressed as the mean ± SD (n = 6/group). (**D**) Caspase 3 activity. Results are expressed as the mean ± SD (n = 6/group). (**E**) Immunoblot analysis of oncogene products and cell cycle regulators. The same sample used in Figure 1A (whole-liver lysate, 50 μg protein) was loaded in each well. The band of actin was used as the loading control. Results are representative of 4 independent experiments. The band intensity was quantified densitometrically, normalized by that of actin, and subsequently normalized by that in *Ppara*$^{+/+}$ nontransgenic mice. The mean value of the fold changes is expressed under each band. (**F**) Immunoblot analysis of phosphorylated ERK1/2 and total ERK1/2. The same samples in Figure 4E (50 μg protein) were used.

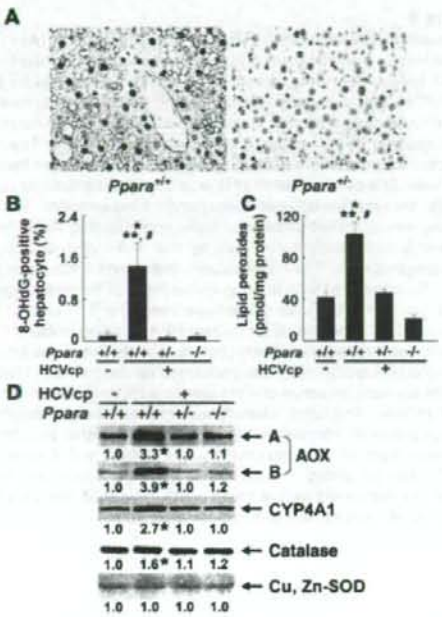

Figure 5
Increased oxidative stress and DNA damage in *Ppara*$^{+/+}$:HCVcpTg mice at 24 months of age. (**A**) Immunohistochemical staining using antibody against 8-OHdG. In *Ppara*$^{+/+}$:HCVcpTg mice, some steatotic hepatocytes were positive for 8-OHdG. Original magnification, ×400. (**B**) Numbers of 8-OHdG–positive hepatocytes. Hepatocyte nuclei stained with anti-8-OHdG antibody were counted in 2,000 hepatocytes of each mouse. Results are expressed as the mean ± SD (n = 6/group). (**C**) Hepatic content of lipid peroxides. Results are expressed as the mean ± SD (n = 6 /group). *P < 0.05 compared with *Ppara*$^{+/+}$ nontransgenic mice; **P < 0.05 compared with *Ppara*$^{+/-}$:HCVcpTg mice; #P < 0.05 compared with *Ppara*$^{-/-}$:HCVcpTg mice. (**D**) Immunoblot analysis of AOX, CYP4A1, catalase, and Cu, Zn-SOD. The whole-liver lysate used in the experiment in Figure 4E (20 μg protein for AOX and CYP4A1 and 50 μg for others) was loaded in each lane. The band of actin was used as the loading control. Results are representative of 4 independent experiments. **A** and **B** indicate full-length and truncated AOX, respectively. The band intensity was quantified densitometrically, normalized by that of actin, and subsequently normalized by that in *Ppara*$^{+/+}$ nontransgenic mice. The mean value of the fold changes is expressed under each band. *P < 0.05 compared with *Ppara*$^{+/+}$ nontransgenic mice.

function. The number of hepatocytes positive for 8-hydroxy-2′-deoxyguanosine (8-OHdG), an indicator of oxidative damage to nuclear DNA, was increased only in 24-month-old *Ppara*$^{+/+}$:HCVcpTg mice (Figure 5, A and B). Lipid peroxides were slightly increased in the livers of 9-month-old *Ppara*$^{+/+}$:HCVcpTg mice (data not shown) and were more abundant in the livers of 24-month-old *Ppara*$^{+/+}$:HCVcpTg mice than in those of *Ppara*$^{+/-}$:HCVcpTg and *Ppara*$^{-/-}$:HCVcpTg mice or *Ppara*$^{+/+}$ nontransgenic mice (Figure 5C). Expression of typical ROS-generating enzymes (AOX and cytochrome P450 4A1 [CYP4A1]) and ROS-eliminating enzymes (catalase and Cu, Zn-SOD) was examined. Immunoblot analysis showed marked increases in the expression of AOX and CYP4A1 and mild increases in that of catalase only in *Ppara*$^{+/+}$:HCVcpTg mice. No changes in Cu, Zn-SOD were found in the subgroups of transgenic mice (Figure 5D). These results suggest that enhanced oxidative stress causes damage in nuclear DNA and probably in mitochondria in the *Ppara*$^{+/+}$:HCVcpTg mice.

Persistent and spontaneous PPARα activation in Ppara$^{+/+}$*:HCVcpTg mice.* Liver tumorigenesis induced by long-term exposure to peroxisome proliferators and the related changes, such as sustained hepatocyte proliferation and increased oxidative stress, are associated with persistent PPARα activation (19–21). To examine the activation of PPARα, we quantified the level of PPARα mRNA, which is induced by PPARα activation (24, 25). PPARα mRNA levels were higher in 9-month-old *Ppara*$^{+/+}$:HCVcpTg mice than in *Ppara*$^{+/+}$ nontransgenic mice (Figure 6A). These increases were more pronounced at 24 months of age. However, there were no differences in PPARα mRNA levels between *Ppara*$^{+/-}$:HCVcpTg and *Ppara*$^{+/-}$ nontransgenic mice at either 9 or 24 months of age. The expression levels of typical PPARα target genes (16, 25, 26) – such as FAT, FATP, L-FABP, AOX, and MCAD (Figure 2); c-Myc, cyclin D1, CDK4, and PCNA (Figure 4); and CYP4A1 (Figure 5) – were simultaneously and synchronously increased in *Ppara*$^{+/+}$:HCVcpTg mice, but not in *Ppara*$^{+/-}$:HCVcpTg or *Ppara*$^{-/-}$:HCVcpTg mice. These results confirm that persistent activation of PPARα occurs only in *Ppara*$^{+/+}$:HCVcpTg mice. Various changes observed in *Ppara*$^{+/+}$:HCVcpTg mice, i.e., increased fatty acid uptake, mitochondrial abnormalities, steatosis, ROS overproduction, accelerated hepatocyte proliferation, and hepatocarcinogenesis, were considered to be closely linked with sustained PPARα activation.

Nuclear PPARα content. The results described above suggest that persistent PPARα activation is critical to the steatogenesis and hepatocarcinogenesis induced by the HCV core protein. A question arises as to why *Ppara*$^{+/-}$:HCVcpTg mice with an active *Ppara* allele do not exhibit the hallmarks of PPARα activation and do not develop HCC. To address this issue, the nuclear PPARα content was analyzed. Immunoblot analysis for PPARα showed that the amount of nuclear PPARα protein in *Ppara*$^{+/+}$:HCVcpTg mice was approximately 2- to 3-fold that of *Ppara*$^{+/+}$ nontransgenic mice, which was disproportionate to the higher PPARα mRNA levels (approximately 1.2- to 1.6-fold) (Figure 6, A and B). The level of nuclear PPARα in *Ppara*$^{+/-}$:HCVcpTg mice was significantly lower than that in *Ppara*$^{+/+}$:HCVcpTg mice and was similar to that in *Ppara*$^{+/+}$ nontransgenic mice (Figure 6B). Thus, the lower amount of nuclear PPARα in *Ppara*$^{+/-}$:HCVcpTg mice than in *Ppara*$^{+/+}$:HCVcpTg mice might have heightened the threshold of expression required for long-term spontaneous PPARα activation.

The degree of an increase in nuclear PPARα levels was evidently higher than the degree of an increase in PPARα mRNA levels in HCVcpTg mice (Figure 6, A and B). To investigate this disparity, the stability of nuclear PPARα was evaluated by pulse-chase experiments using isolated hepatocytes obtained from these mice. The half-life of nuclear PPARα was significantly longer (P < 0.05) in *Ppara*$^{+/+}$:HCVcpTg mice (11.5 ± 2.3 h) than in *Ppara*$^{+/+}$ nontransgenic mice (5.8 ± 1.4 h) (Figure 6C). The half-life of nuclear PPARα in *Ppara*$^{+/-}$:HCVcpTg mice tended to be prolonged compared with that in *Ppara*$^{+/-}$ nontransgenic mice (Figure 6C). These results suggest that the stability of nuclear PPARα was increased as a result of HCV core protein expression. Because it is known that the core protein interacts with retinoid X receptor α (RXRα) (27) and that

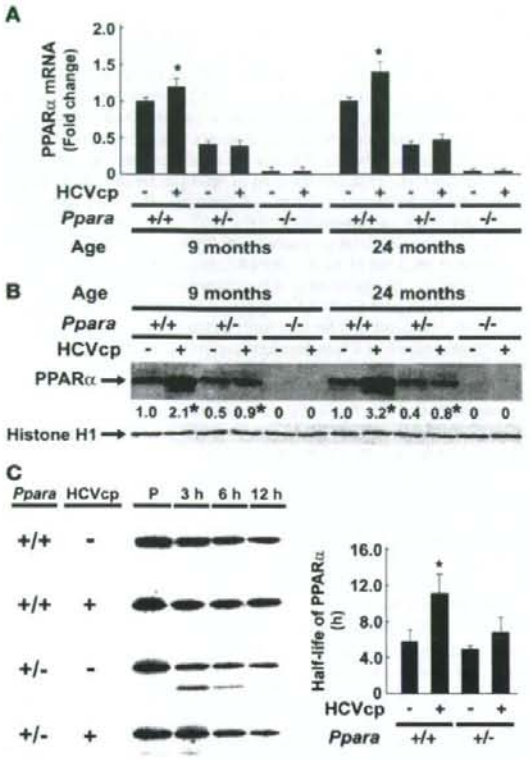

Figure 6
Persistent PPARα activation in *Ppara*$^{+/+}$:HCVcpTg mice. (**A**) PPARα mRNA levels. Total RNA was prepared from each mouse, and PPARα mRNA levels were determined by RT-PCR, normalized by those of GAPDH, and subsequently normalized by those of 9-month-old *Ppara*$^{+/+}$ nontransgenic mice. Results are expressed as the mean ± SD (n = 6 /group). (**B**) Immunoblot analysis of nuclear PPARα. The nuclear fraction obtained from each mouse (100 μg protein) was loaded in each well. The band of histone H1 was used as the loading control. Results are representative of 6 independent experiments. The band intensity was quantified densitometrically, normalized by that of histone H1, and subsequently normalized by that in 9-month-old *Ppara*$^{+/+}$ nontransgenic mice. The mean value is expressed under each band. *P < 0.05 compared with nontransgenic mice of the same age and *Ppara* genotype. (**C**) Pulse-chase experiments for 3, 6, and 12 h and pulse-label (P) experiments for nuclear PPARα using isolated mouse hepatocytes. Left: labeled PPARα bands on x-ray film. Pulse-label and pulse-chase experiments were performed as described in Methods. Results are representative of 4 independent experiments. Right: half-life of PPARα. The band intensity was measured densitometrically and subsequently normalized by that of the pulse-label experiments. The percentage of the band intensity was plotted, and the half-life of PPARα was calculated. Results obtained from 4 independent experiments are expressed as the mean ± SD. *P < 0.05 compared with nontransgenic mice in the same *Ppara* genotype.

PPARα influences the stability of RXRα (28), it is plausible that the core protein would affect its action in nuclei through an interaction with the PPARα-RXRα heterodimer and stabilization of PPARα.

Development of hepatic steatosis and HCC with long-term clofibrate treatment in Ppara$^{+/-}$*:HCVcpTg mice.* To further confirm the significance of persistent PPARα activation on core protein–induced pathological changes, *Ppara*$^{+/-}$ and *Ppara*$^{+/-}$:HCVcpTg mice were fed a standard diet containing 0.05% clofibrate for 24 months. Interestingly, hepatic steatosis appeared in the clofibrate-treated *Ppara*$^{+/-}$:HCVcpTg mice, but not in the *Ppara*$^{+/-}$ mice under the same treatment conditions (Figure 7, A and B). Similar to our observations in *Ppara*$^{+/+}$:HCVcpTg mice not treated with clofibrate, aberrant mitochondria with discontinuous outer membranes and decreased palmitic acid β-oxidation activity were found only in the clofibrate-treated *Ppara*$^{+/-}$:HCVcpTg mice (Figure 7, A and C). In addition, levels of MCAD mRNA; AOX, and CYP4A1 proteins; PPARα mRNA; and nuclear PPARα protein were higher in the clofibrate-treated *Ppara*$^{+/-}$:HCVcpTg mice than in the clofibrate-treated *Ppara*$^{+/-}$ mice (Figure 7, D–F), which suggests that the degree of PPARα activation in the former group was greater than that in the latter group and similar to that in *Ppara*$^{+/+}$:HCVcpTg mice not treated with clofibrate. Finally, the incidence of HCC after clofibrate treatment was higher in *Ppara*$^{+/-}$:HCVcpTg mice (25%; 5 in 20 mice) than in *Ppara*$^{+/-}$ mice (5%; 1 in 20 mice). Therefore, these results corroborate the importance of constant PPARα activation to the pathogenesis of hepatic steatosis and HCC in the transgenic mice.

Discussion

A novel and striking finding in this study is the absolute requirement of persistent PPARα activation for the development of HCV core protein–induced steatosis and HCC. Our data also show that the HCV core protein alone cannot induce steatosis and HCC in transgenic mice.

Mechanisms of development of steatosis in HCVcpTg mice were previously explained as an enhancement of de novo synthesis of fatty acids (29) and a decrease in MTP expression, the latter of which results in insufficient VLDL secretion from hepatocytes (30). In the present study, we revealed 2 novel mechanisms of steatogenesis in the transgenic mice, i.e., an impairment of mitochondrial β-oxidation due to the breakdown of mitochondrial outer membranes and an increase in fatty acid uptake into hepatocytes, associated with PPARα activation. PPARα activation, mitochondrial dysfunction, and hepatic steatosis appeared in 9-month-old *Ppara*$^{+/+}$:HCVcpTg mice and continued until 24 months of age, clearly preceding development of HCC. These findings thereby indicate a correlation between PPARα activation, hepatic steatosis, and HCC.

We obtained the novel and rather paradoxical finding that significant PPARα activation, which generally is expected to reduce hepatic triglyceride levels, is essential for the development of severe steatosis induced by HCV core protein. According to the results of this study, the following hypothesis concerning the development of steatosis in *Ppara*$^{+/+}$:HCVcpTg mice is proposed. First, the HCV core protein localizes partly in mitochondria (9). A recent study

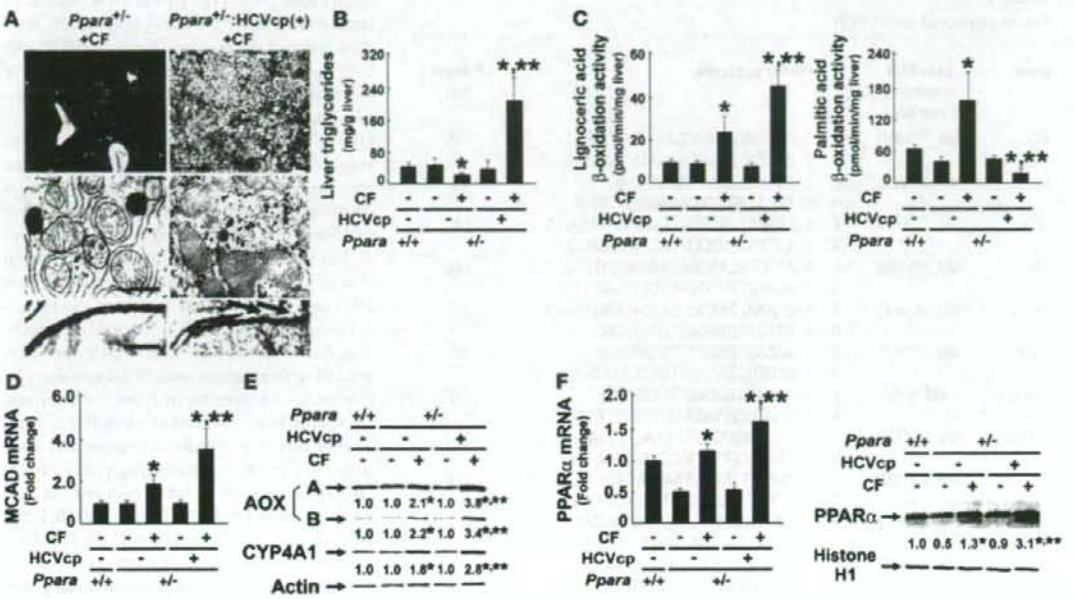

Figure 7

Development of hepatic steatosis by long-term treatment of clofibrate in *Ppara*$^{+/-}$:HCVcpTg mice. (**A**) Histological examination of *Ppara*$^{+/-}$ and *Ppara*$^{+/-}$:HCVcpTg mice treated with diet containing 0.05% (w/w) clofibrate for 24 months (CF). Top: Histological appearance of H&E-stained liver sections. Magnification, ×40. Microvesicular and macrovesicular steatosis were detected only in clofibrate-treated *Ppara*$^{+/-}$:HCVcpTg mice. Middle and bottom: Electron microscopic features of hepatic mitochondria. Some C-shaped mitochondria showing discontinuance of outer membranes (arrows) were found in clofibrate-treated *Ppara*$^{+/-}$:HCVcpTg mice. Scale bars: 400 nm (middle), 30 nm (bottom). (**B** and **C**) Content of liver triglycerides and lignoceric and palmitic acid β-oxidation activities. (**D**) MCAD mRNA levels. mRNA levels were normalized to those of GAPDH and subsequently normalized to those in *Ppara*$^{+/+}$ nontransgenic mice. (**E**) Immunoblot analysis of AOX and CYP4A1. Whole-liver lysate (20 μg protein) was loaded in each lane. Actin was used as a loading control. Results are representative of 6 independent experiments. (**F**) PPARα mRNA levels and nuclear PPARα contents. Left: PPARα mRNA levels. The same samples used in **D** were adopted. Right: Immunoblot analysis of nuclear PPARα. Nuclear fraction obtained from each mouse (100 μg protein) was loaded in each well. Histone H1 was used as a loading control. In **E** and **F**, the mean value of the fold changes is shown under each band. Results are representative of 6 independent experiments. Band intensity was quantified densitometrically, normalized to that of the loading control, and subsequently normalized to that in *Ppara*$^{+/+}$ nontransgenic mice. *$P < 0.05$ compared with untreated mice of the same genotype; **$P < 0.05$ compared with clofibrate-treated *Ppara*$^{+/-}$ mice without core protein gene. Results are expressed as mean ± SD ($n = 6$/group).

showed that, in isolated mitochondria, the core protein directly increased Ca^{2+} influx, inhibited electron transport complex I activity, and induced ROS production (31), all of which can increase the fragility of mitochondria and depress mitochondrial function. In addition, the HCV core protein also localizes in nuclei (9) and can coexist in PPARα-RXRα heterodimer through a direct interaction with the DNA-binding domain of RXRα, which enhances the transcriptional activity of PPARα target genes, such as AOX, despite the absence of PPARα ligands in cultured cells (27). The HCV core protein can also be involved in the PPARα-RXRα complex through a direct interaction with cyclic-AMP responsive element binding protein-binding protein (32), which is able to bind to PPARα (33). Thus, the core protein probably serves as a coactivator and stabilizer of PPARα in vivo, which was further confirmed in this study. Moreover, because it is also known that the core protein itself activates ERK1/2 and p38 mitogen-activated protein kinase (34), these activations might phosphorylate PPARα and thereby transactivate it (35). The core protein–induced PPARα activation enhances the basal expression of AOX and CYP4A1, which leads to increased production of ROS and dicarboxylic acids. These toxic compounds can damage mitochondrial outer membranes, which impairs the mitochondrial β-oxidation system. These damages directly induce the accumulation of long-chain fatty acids in hepatocytes. Furthermore, PPARα activation increases the expression of FAT and FATP, which promotes the influx of fatty acids from blood. Long-chain fatty acids and their CoA esters accumulated in hepatocytes are likely to act as potent detergents, which further damages the outer membranes of mitochondria. Fatty acids and their derivatives function as natural ligands of PPARα, which results in the activation of PPARα and the induction of FAT, FATP, AOX, and CYP4A1, which further accelerates mitochondrial damage, the reduction of mitochondrial β-oxidation activity, and the accumulation of fatty acids in a vicious cycle.

Persistent PPARα activation increases oxidative DNA damage because of a disproportionate increase in ROS-generating enzymes relative to the levels of degrading enzymes such as catalase and SOD, which can predispose hepatocytes to malignant transformation. In addition, persistent PPARα activation leads to increased

Table 2
Primer pairs used for RT-PCR

Gene	GeneBank accession number		Primer sequence	Product (bp)
ACC	NM_133360	F	5′-GGGCACAGACCGTGGTAGTT-3′	105
		R	5′-CAGGATCAGCTGGGATACTGAGT-3′	
ApoB	NM_009693	F	5′-TCACCCCCGGGATCAAG-3′	85
		R	5′-TCCAAGGACACAGAGGGCTTT-3′	
AOX	NM_015729	F	5′-TGGTATGGTGTCGTACTTGAATGAC-3′	145
		R	5′-AATTTCTACCAATCTGGCTGCAC-3′	
FAS	NM_007988	F	5′-ATCCTGGAACGAGAACACGATCT-3′	140
		R	5′-AGAGACGTGTCACTCCTGGACTT-3′	
FAT	NM_007643	F	5′-CCAAATGAAGATGAGCATAGGACAT-3′	87
		R	5′-GTTGACCTGCAGTCGTTTTGC-3′	
FATP	NM_011977	F	5′-ACCACCGGGCTTCCTAAGG-3′	80
		R	5′-CTGTAGGAATGGTGGCCAAAG-3′	
GAPDH	M32599	F	5′-TGCACCACCAACTGCTTAG-3′	177
		R	5′-GGATGCAGGGATGATGTTCTG-3′	
L-FABP	NM_017399	F	5′-GCAGAGCCAGGAGAACTTTGAG-3′	121
		R	5′-TTTGATTTTCTTCCCTTCATGCA-3′	
MCAD	NM_007382	F	5′-TGCTTTTGATAGAACCAGACCTACAGT-3′	128
		R	5′-CTTGGTGCTCCACTAGCAGCTT-3′	
MTP	NM_008642	F	5′-GAGCGGTCTGGATTTACAACG-3′	72
		R	5′-GTAGGTAGTGACAGATGTGGCTTTTG-3′	
PPARα	NM_011144	F	5′-CCTCAGGGTACCACTACGGAGT-3′	69
		R	5′-GCCGAATAGTTCGCCGAA-3′	

F, forward sequence; R, reverse sequence.

cell division, as revealed by the expression of cell cycle regulators such as cyclin D1 and CDK4. Furthermore, there is little change in apoptosis, which, under normal circumstances, would remove damaged cells capable of undergoing transformation. Thus, under these conditions, it is plausible that some aberrant hepatocytes do not undergo apoptosis and develop into HCC.

It is well known that chronic activation of PPARα is associated with hepatocarcinogenesis in mice exposed to peroxisome proliferators or in mice lacking AOX expression. The common clinicopathological characteristics of HCC in these mice are multicentric HCC (20, 22, 36, 37), the well-differentiated appearance of HCC including trabecular features and often a "nodule-in-nodule" pattern (22, 36, 37), and no evidence of fibrosis or cirrhosis in the nonneoplastic liver parenchyma (22, 36), similar to that observed in *Ppara*$^{+/+}$:HCVcpTg mice. However, mice chronically exposed to peroxisome proliferators are clearly distinct from *Ppara*$^{+/+}$:HCVcpTg mice in that they have normal mitochondrial organization, increased mitochondrial β-oxidation activity, and no steatosis (16, 36). AOX-null mice are also different from *Ppara*$^{+/+}$:HCVcpTg mice with respect to mitochondrial structure (22). These detailed comparisons between the 3 mouse models reveal the importance of mitochondrial abnormalities in the pathogenesis of HCV-related diseases.

PPARα is known to regulate the hepatic expression of many proteins associated with fatty acid and triglyceride metabolism, cell division and apoptosis, oxidative stress generation and degradation, and so forth (15, 16, 20, 21, 24–26); therefore, complete deletion of the PPARα gene from mice might cause hitherto unknown influences on the pathways involved in the development of hepatic steatosis and HCC. To consider these unknown effects, *Ppara*$^{+/-}$:HCVcpTg mice were adopted in the current study. Surprisingly, almost all results from *Ppara*$^{+/-}$:HCVcpTg mice were similar to those from *Ppara*$^{-/-}$:HCVcpTg mice, which demonstrates that the presence of functional PPARα itself is not a prerequisite for the occurrence of steatosis and HCC induced by the HCV core protein. Moreover, a comparison between *Ppara*$^{+/-}$:HCVcpTg and *Ppara*$^{+/+}$:HCVcpTg mice uncovered an unexpected and important fact that the core protein–dependent pathological changes do not appear without significant activation of PPARα. Thus, it is not the presence of PPARα per se, but rather a high level of PPARα activation that seems to be essential for the development of HCV core protein–induced steatosis and HCC.

To reinforce the abovementioned hypothesis, *Ppara*$^{+/-}$ and *Ppara*$^{+/-}$:HCVcpTg mice were treated with an exogenous PPAR agonist, clofibrate, for 24 months. In *Ppara*$^{+/-}$ mice, long-term clofibrate treatment caused a certain level of persistent PPARα activation and a low incidence of HCC. Interestingly, in *Ppara*$^{+/-}$:HCVcpTg mice, clofibrate treatment induced more intensive PPARα activation and HCC at a much higher incidence, accompanied by damaged mitochondrial outer membranes, severe steatosis, and decreased mitochondrial β-oxidation activity. The results from the clofibrate-treated *Ppara*$^{+/-}$:HCVcpTg mice were similar to those of the *Ppara*$^{+/+}$:HCVcpTg mice not treated with clofibrate. Therefore, these findings further support the concept that a long-term and high level of PPARα activation is necessary for steatogenesis and hepatocarcinogenesis in HCVcpTg mice and emphasize the significant role of the HCV core protein as a PPARα coactivator in vivo.

A pulse-chase experiment showed that PPARα was stabilized in hepatocyte nuclei in mice expressing the HCV core protein. Many nuclear receptors, including PPARα and RXRα, are known to be degraded by the ubiquitin-proteasome system (38), which plays an important role in modulating the activity of nuclear receptors. Further studies will be needed to clarify whether the core protein influences the ubiquitin-proteasome pathway.

Recent studies have shown conflicting result, i.e., that PPARα was downregulated in the livers of chronic hepatitis C patients (39, 40). Although the association between PPARα function and chronic HCV infection remains a matter of controversy in humans, the changes observed in the transgenic mice resemble in many ways the clinicopathological features of chronically HCV-infected patients; both show a high frequency of accompanying steatosis (10, 40, 41), increased accumulation of carbon 18 monounsaturated fatty acids in the liver (42), mitochondrial dysfunction (43), increased insulin resistance (44) and oxidative stress (45, 46), male-preferential (2) and multicentric occurrence of HCC (47, 48), and the well-differentiated appearance of HCC, including trabecular features and often a "nodule-in-nodule" pattern (47, 48). Thus, it is postulated that the mechanism of steatogenesis and hepatocarcinogenesis we proposed may partially apply to patients with chronic HCV infection. If so, therapeutic interventions to alleviate persistent and excessive PPARα activation might be beneficial in the prevention of HCC. To clarify the exact relationship between PPARα activation and HCV-induced hepatocarcinogenesis in humans, further

experiments using noncancerous liver tissues obtained from HCV-related HCC patients and using mice carrying human PPARα and HCV core protein genes are needed.

In conclusion, we clarified for the first time that persistent and potent PPARα activation is absolutely required for the development of severe steatosis and HCC induced by HCV core protein. In addition, we uncovered paradoxical and specific functions of PPARα in the mechanism of steatogenesis mediated by the core protein. Our results offer clues in the search for novel therapeutic and nutritional management options, especially with respect to neutral lipids, for chronically HCV-infected patients.

Methods

Mice. The generation of HCVcpTg mice and *Ppara*$^{-/-}$ mice was described previously (7, 24, 49). Male HCVcpTg mice and female *Ppara*$^{-/-}$ mice were mated, and F1 mice bearing the HCV core protein gene were intercrossed to produce F2 mice. *Ppara*$^{+/+}$, *Ppara*$^{+/-}$, and *Ppara*$^{-/-}$ mice bearing the HCV core protein gene, designated as *Ppara*$^{+/+}$:HCVcpTg, *Ppara*$^{+/-}$:HCVcpTg, and *Ppara*$^{-/-}$:HCVcpTg mice, in the F4 generation were subjected to serial analyses. Because HCC develops preferentially in male HCVcpTg mice (9), male mice were analyzed. Age-matched male *Ppara*$^{+/+}$ mice without the core protein gene were used as controls. For identifying genotypes, genomic DNA was isolated from mouse tails and amplified by PCR. Primer pairs were designed as described elsewhere: 5′-GCCCACAGGACGTTAAGTTC-3′ and 5′-TAGTTCACGCCGTCCTCCAG-3′ for the HCV core gene (7) and 5′-CAGAGCAACCATCCAGATGA-3′ and 5′-AAACGCAACGTAGAGTGCTG-3′ for the PPARα gene (24). Amplified alleles for HCV core and PPARα genes were 460 and 472 base pairs, respectively. Five mice per cage were fed a routine diet and were kept free of specific pathogens according to institutional guidelines. For the clofibrate treatment experiments, 2-month-old male *Ppara*$^{+/+}$ and *Ppara*$^{+/+}$:HCVcpTg mice were randomly divided into 2 groups (n = 20 in each group) and were fed either a routine diet or one containing 0.05% (w/w) clofibrate (Wako Pure Chemicals Industries) for 24 months. All mice were killed by cervical dislocation before their livers were excised. If a hepatic tumor was present, the tumor was removed and subjected to histological analysis, and the remaining liver tissues were used for biochemical analyses. All animal experiments were conducted in accordance with animal study protocols outlined in the *Guide for the Care and Use of Laboratory Animals* prepared by the National Academy of Sciences and approved by the Shinshu University School of Medicine.

Preparation of nuclear, mitochondrial, and cytosolic fractions. Approximately 400 mg of liver tissue was minced on ice and transferred to 10% (w/v) isolation buffer (250 mM sucrose in 10 mM Tris-HCl [pH 7.4] and 0.5 mM EGTA and 0.1% bovine serum albumin [pH 7.4]). The samples were gently homogenized by 10–20 strokes with a chilled Dounce homogenizer (Wheaton) and loose-fitting pestle. The homogenate was centrifuged at 500 × *g* for 5 min at 4°C. The supernatant was retained, and the resulting pellet was resuspended with isolation buffer and centrifuged at 4,500 *g* for 10 min at 4°C. The pellet fraction was suspended again and centrifuged at 20,000 × *g* for 1 h at 4°C, and the resulting pellet was used as the nuclear fraction. The combined supernatant fractions were centrifuged at 7,800 × *g* for 10 min at 4°C to obtain a crude mitochondria pellet. This pellet was resuspended with isolation buffer, centrifuged at 7,800 × *g* for 10 min at 4°C, and used as the mitochondrial fraction. Finally, all supernatant fractions were collected and centrifuged at 20,000 × *g* for 30 min at 4°C, and the resulting supernatant was used as the cytosolic fraction.

Immunoblot analysis. Protein concentrations were measured colorimetrically with a BCA Protein Assay kit (Pierce). For the analysis of fatty acid–metabolizing enzymes, hepatocyte mitochondrial fractions or whole-liver lysates (20 μg protein) were subjected to 10% SDS-PAGE (16). For analysis of PPARα, nuclear fractions (100 μg protein) were used. For analysis of other proteins, whole lysates or cytosolic fractions (50 μg protein) were subjected to electrophoresis. After electrophoresis, the proteins were transferred to nitrocellulose membranes, which were incubated with the primary antibody and then with alkaline phosphatase–conjugated goat anti-rabbit or anti-mouse IgG. Antibodies against HCV core protein, fatty acid–metabolizing enzymes, CYP4A1, catalase, and PPARα were described previously (9, 16, 24, 50). Antibodies against other proteins were purchased commercially: cytochrome *c* antibody from BD Transduction Laboratories and other antibodies from Santa Cruz Biotechnology. The band of actin or histone H1 was used as the loading control. The band intensity was measured densitometrically, normalized to that of actin or histone H1, and subsequently expressed as fold changes relative to that of *Ppara*$^{+/+}$ nontransgenic mice.

Analysis of mRNA. Total liver RNA was extracted using an RNeasy Mini Kit (Qiagen), and cDNA was generated by SuperScript II reverse transcriptase (Gibco BRL). Quantitative RT-PCR was performed using a SYBR green PCR kit and an ABI Prism 7700 Sequence Detection System (Applied Biosystems). The primer pairs used for RT-PCR are shown in Table 2. The mRNA level was normalized to the GAPDH mRNA level and subsequently expressed as fold changes relative to that of *Ppara*$^{+/+}$ nontransgenic mice.

Light microscopy and immunohistochemical analysis. Small blocks of liver tissue from each mouse were fixed in 10% formalin in phosphate-buffered saline and embedded in paraffin. Sections (4 μm thick) were stained with hematoxylin and eosin. For immunohistochemical localization of PCNA and 8-OHdG, other small blocks of liver tissue were fixed in 4% paraformaldehyde in phosphate-buffered saline. Sections (4 μm thick) then were affixed to glass slides and incubated overnight with mouse monoclonal antibodies against PCNA (1:100 dilution; Santa Cruz) or 8-OHdG (1:10 dilution; Japan Institute for the Control of Aging). Sections were immunostained using EnVision+ kit, with 3,3′-diaminobenzidine as a substrate (DAKO). Hepatocytes positive for PCNA or 8-OHdG were examined in 10 randomly selected ×400 microscopic fields per section. Two-thousand hepatocytes were examined for each mouse, and the number of immunostained hepatocyte nuclei was expressed as a percentage.

Assessment of hepatocyte apoptosis. TUNEL assay was performed using a MEBSTAIN Apoptosis Kit II (Medical & Biological Laboratories). Two thousand hepatocytes were examined for each mouse, and the number of TUNEL-positive hepatocytes was expressed as a percentage.

Pulse-label and pulse-chase experiments. Parenchymal hepatocytes were isolated by the modified *in situ* perfusion method (51). After perfusion with 0.05% collagenase solution (Wako), the isolated hepatocytes were washed 3 times by means of differential centrifugation and the dead cells were removed by density-gradient centrifugation at 500 *g* for 3 min at 4°C on Percoll (Amersham Pharmacia Biotech). The live hepatocytes were washed and suspended in William's E medium containing 5% FBS. When the viability of the isolated hepatocytes exceeded 85% as determined by the trypan blue exclusion test, the following experiments were conducted. The isolated hepatocytes were washed twice and incubated in methionine-free medium containing 5% dialyzed FBS for 1 h at 37°C. The medium was replaced with the same medium containing 300 mCi/ml of [^{35}S]methionine (Amersham Pharmacia Biotech). After a 3-h incubation, the labeled medium was exchanged for the standard medium, and the preparation was chased for 3, 6, or 12 h. The labeled cells were washed, homogenized, and centrifuged at 800 *g* for 5 min at 4°C to obtain a crude nucleus pellet. This pellet was resuspended with isolation buffer and centrifuged at 20,000 *g* for 1 h at 4°C to prepare the nuclear fraction. The levels of radioactivity in the homogenates of the pulse-labeled preparations were similar between the transgenic and the nontransgenic mice, which suggested that the [^{35}S]methionine uptake capacity in the former hepatocytes was similar to that in the latter. The nuclear fraction was lysed in RIPA buffer (10 mM Tris-HCl, pH 7.4; 0.2% sodium deoxycholate, 0.2% Nonidet P-40, 0.1% SDS,

0.25 mM PMSF, and 10 mg/ml aprotinin). The lysate was incubated for 3 h at 4°C with purified anti-PPARα antibody. The immune complexes were precipitated with *Staphylococcus aureus* protein A bound to agarose beads. After the precipitates had been washed in RIPA buffer, the labeled proteins were resolved by 10% SDS-PAGE and visualized by autoradiography.

Analysis of fatty acid uptake ability. Assays for fatty acid uptake were carried out according to a method reported by Graulet et al. (52) with minor modifications. Briefly, 3 mice in each group were fasted overnight. Livers were removed quickly, rinsed in ice-cold saline solution, and cut into 500-μm thick slices with an Oxford Vibratome (Oxford Laboratories). Approximately 150 mg of fresh liver (6–8 liver slices) was placed on stainless steel grids positioned in a 25-ml flask equipped with suspended plastic center wells (Kontes) and incubated in RPMI-1640 medium (Sigma-Aldrich) devoid of fatty acids for 2 h at 37°C. The medium was then replaced with fresh RPMI-1640 medium supplemented with an antibiotic-antimycotic cocktail and 0.8 mM [1-^{14}C]palmitic acid (4 mCi/mmol) (American Radiolabeled Chemicals) complexed to BSA (palmitic acid:albumin molar ratio of 4:1). After a 7-h incubation, the medium was collected and slices were washed with 2 ml of saline solution and homogenized in Tris buffer (25 mM Tris-HCl, pH 8.0; 50 mM NaCl). Fatty acid uptake ability was calculated as the sum of palmitic acid converted to CO_2 and ketone bodies with that incorporated into total cellular lipids after incubation. For measurement of CO_2 production by the liver slices, the center wells were placed into scintillation vials containing 4 ml of scintillation cocktail, and radioactivity was counted. For measurement of ketone body generation, aliquots of medium (500 μl) and liver homogenates (250 μl) were treated with ice-cold perchloric acid to make final concentrations of 200 mM and were centrifuged at 3,000 *g* for 20 min at 4°C. Aliquots of the supernatant containing the ketone bodies were introduced into the scintillation vials, and radioactivity was counted. Total cellular lipids were extracted from the liver homogenates according to a modified method developed by Folch et al. (53), collected into scintillation vials, and evaporated to dryness under an air stream; radioactivity was then counted. The experiment was repeated 3 times, and palmitic acid uptake ability was expressed as fold changes relative to that of *Ppara*$^{-/-}$ nontransgenic mice.

Other methods. To determine the hepatic content of lipids and lipid peroxides, lipids were extracted according to a method by Folch et al. (53). Triglycerides and free fatty acids were measured with a Triglyceride E-test kit and a NEFA C-test kit (Wako), respectively. Lipid peroxides (malondialdeyde and 4-hydroxyalkenals) were measured using an LPO-586 kit (OXIS International). Hepatic β-oxidation activity was determined as described previously (16). Hepatic caspase 3 activity was measured as described elsewhere (54). Plasma glucose and insulin levels were determined using a Glucose CII-test kit (Wako) and a mouse insulin ELISA kit (U-type, AKRIN-031; Shibayagi), respectively.

Statistics. Statistical analysis was performed with a 2-tailed Student's *t* test for quantitative variables or with a chi-square test for qualitative variables. Quantitative data are expressed as the mean ± SD. $P < 0.05$ was considered to be statistically significant.

Acknowledgments

We thank Trevor Ralph for editorial assistance and Chikako Tanaka for helpful suggestions.

Received for publication August 13, 2007, and accepted in revised form November 7, 2007.

Address correspondence to: Naoki Tanaka, Department of Metabolic Regulation, Institute on Aging and Adaptation, Shinshu University Graduate School of Medicine, Asahi 3-1-1, Matsumoto 390-8621, Japan. Phone: 81-263-37-2850; Fax: 81-263-37-3094; E-mail: naopi@hsp.md.shinshu-u.ac.jp.

1. Kiyosawa, K., et al. 1990. Interrelationship of blood transfusion, non-A, non-B hepatitis and hepatocellular carcinoma: analysis by detection of antibody to hepatitis C virus. *Hepatology.* **12**:671–675.
2. Kiyosawa, K., et al. 2004. Hepatocellular carcinoma: recent trends in Japan. *Gastroenterology.* **127**(5 Suppl. 1):S17–S26.
3. Tanaka, Y., et al. 2002. Inaugural article: a comparison of the molecular clock of hepatitis C virus in the United States and Japan predicts that hepatocellular carcinoma incidence in the United States will increase over the next two decades. *Proc. Natl. Acad. Sci. U. S. A.* **99**:15584–15589.
4. Okuda, K., Fujimoto, I., Hanai, A., and Urano, Y. 1987. Changing incidence of hepatocellular carcinoma in Japan. *Cancer Res.* **47**:4967–4972.
5. El-Serag, H.B., and Mason, A.C. 1999. Rising incidence of hepatocellular carcinoma in the United States. *N. Engl. J. Med.* **340**:745–750.
6. Shimotohno, K. 2000. Hepatitis C virus and its pathogenesis. *Semin. Cancer Biol.* **10**:233–240.
7. Moriya, K., et al. 1997. Hepatitis C virus core protein induces hepatic steatosis in transgenic mice. *J. Gen. Virol.* **78**:1527–1531.
8. Shintani, Y., et al. 2004. Hepatitis C virus infection and diabetes: direct involvement of the virus in the development of insulin resistance. *Gastroenterology.* **126**:840–848.
9. Moriya, K., et al. 1998. The core protein of hepatitis C virus induces hepatocellular carcinoma in transgenic mice. *Nat. Med.* **4**:1065–1068.
10. Powell, E.E., Jonsson, J.R., and Clouston, A.D. 2005. Steatosis: co-factor in other liver diseases. *Hepatology.* **42**:5–13.
11. Ohata, K., et al. 2003. Hepatic steatosis is a risk factor for hepatocellular carcinoma in patients with chronic hepatitis C virus infection. *Cancer.* **97**:3036–3043.
12. Browning, J.D., and Horton, J.D. 2004. Molecular mediators of hepatic steatosis and liver injury. *J. Clin. Invest.* **114**:147–152.
13. Le, T.H., et al. 2004. The zonal distribution of megamitochondria with crystalline inclusions in nonalcoholic steatohepatitis. *Hepatology.* **39**:1423–1429.
14. Yang, S., Lin, H.Z., Hwang, J., Chacko, V.P., and Diehl, A.M. 2001. Hepatic hyperplasia in noncirrhotic fatty livers: is obesity-related hepatic steatosis a premalignant condition? *Cancer Res.* **61**:5016–5023.
15. Desvergne, B., and Wahli, W. 1999. Peroxisome proliferator-activated receptors: nuclear control of metabolism. *Endocr. Rev.* **20**:649–688.
16. Aoyama, T., et al. 1998. Altered constitutive expression of fatty acid-metabolizing enzymes in mice lacking the peroxisome proliferator-activated receptor α (PPARα). *J. Biol. Chem.* **273**:5678–5684.
17. Staels, B., et al. 1998. Mechanism of action of fibrates on lipid and lipoprotein metabolism. *Circulation.* **98**:2088–2093.
18. Harano, Y., et al. 2006. Fenofibrate, a peroxisome proliferator-activated receptor α agonist, reduces hepatic steatosis and lipid peroxidation in fatty liver Shionogi mice with hereditary fatty liver. *Liver Int.* **26**:613–620.
19. Yeldandi, A.V., Rao, M.S., and Reddy, J.K. 2000. Hydrogen peroxide generation in peroxisome proliferator-induced oncogenesis. *Mutat. Res.* **448**:159–177.
20. Yu, S., Rao, M.S., and Reddy, J.K. 2003. Peroxisome proliferator-activated receptors, fatty acid oxidation, steatohepatitis and hepatocarcinogenesis. *Curr. Mol. Med.* **3**:561–572.
21. Peters, J.M., Cattley, R.C., and Gonzalez, F.J. 1997. Role of PPARα in the mechanism of action of the nongenotoxic carcinogen and peroxisome proliferator Wy-14,643. *Carcinogenesis.* **18**:2029–2033.
22. Fan, C.Y., et al. 1998. Steatohepatitis, spontaneous peroxisome proliferation and liver tumors in mice lacking peroxisomal fatty acyl-CoA oxidase. Implications for peroxisome proliferator-activated receptor α natural ligand metabolism. *J. Biol. Chem.* **273**:15639–15645.
23. Moriya, K., et al. 2001. Oxidative stress in the absence of inflammation in a mouse model for hepatitis C virus-associated hepatocarcinogenesis. *Cancer Res.* **61**:4365–4370.
24. Lee, S.S., et al. 1995. Targeted disruption of the α isoform of the peroxisome proliferator-activated receptor gene in mice results in abolishment of the pleiotropic effects of peroxisome proliferators. *Mol. Cell. Biol.* **15**:3012–3022.
25. Mandard, S., Muller, M., and Kersten, S. 2004. Peroxisome proliferator-activated receptor α target genes. *Cell. Mol. Life Sci.* **61**:393–416.
26. Peters, J.M., et al. 1998. Role of peroxisome proliferator-activated receptor α in altered cell cycle regulation in mouse liver. *Carcinogenesis.* **19**:1989–1994.
27. Tsutsumi, T., et al. 2002. Interaction of hepatitis C virus core protein with retinoid X receptor α modulates its transcriptional activity. *Hepatology.* **35**:937–946.
28. Tanaka, N., et al. 2003. In vivo stabilization of nuclear retinoid X receptor α in the presence of peroxisome proliferator-activated receptor α. *FEBS Lett.* **543**:120–124.
29. Moriishi, K., et al. 2007. Critical role of PA28γ in hepatitis C virus-associated steatogenesis and hepatocarcinogenesis. *Proc. Natl. Acad. Sci. U. S. A.* **104**:1661–1666.
30. Perlemuter, G., et al. 2002. Hepatitis C virus core

protein inhibits microsomal triglyceride transfer protein activity and very low density lipoprotein secretion: a model of viral-related steatosis. *FASEB J.* **16**:185–194.
31. Korenaga, M., et al. 2005. Hepatitis C virus core protein inhibits mitochondrial electron transport and increases reactive oxygen species (ROS) production. *J. Biol. Chem.* **280**:37481–37488.
32. Gomez-Gonzalo, M., et al. 2004. Hepatitis C virus core protein regulates p300/CBP co-activation function. Possible role in the regulation of NF-AT1 transcriptional activity. *Virology.* **328**:120–130.
33. Yu, S., and Reddy, J.K. 2007. Transcription coactivators for peroxisome proliferator-activated receptors. *Biochim. Biophys. Acta.* **1771**:936–951.
34. Spaziani, A., Alisi, A., Sanna, D., and Balsano, C. 2006. Role of p38 MAPK and RNA-dependent protein kinase (PKR) in hepatitis C virus core-dependent nuclear delocalization of cyclin B1. *J. Biol. Chem.* **281**:10983–10989.
35. Diradourian, C., Girard, J., and Pegorier, J.P. 2005. Phosphorylation of PPARs: from molecular characterization to physiological relevance. *Biochimie.* **87**:33–38.
36. Reddy, J.K., Rao, M.S., Azarnoff, D.L., and Sell, S. 1979. Mitogenic and carcinogenic effects of a hypolipidemic peroxisome proliferator, [4-chloro-6-(2,3-xylidino)-2- pyrimidinylthio]acetic acid (Wy-14,643), in rat and mouse liver. *Cancer Res.* **39**:152–161.
37. Rao, M.S., and Reddy, J.K. 1996. Hepatocarcinogenesis of peroxisome proliferators. *Ann. N. Y. Acad. Sci.* **804**:573–587.
38. Genini, D., and Catapano, C.V. 2006. Control of peroxisome proliferator-activated receptor fate by the ubiquitin-proteasome system. *J. Recept. Signal. Transduct. Res.* **26**:679–692.
39. Dharancy, S., et al. 2005. Impaired expression of the peroxisome proliferator-activated receptor alpha during hepatitis C virus infection. *Gastroenterology.* **128**:334–342.
40. de Gottardi, A., et al. 2006. Peroxisome proliferator-activated receptor-alpha and -gamma mRNA levels are reduced in chronic hepatitis C with steatosis and genotype 3 infection. *Aliment. Pharmacol. Ther.* **23**:107–114.
41. Lefkowitch, J.H., et al. 1993. Pathological diagnosis of chronic hepatitis C: a multicenter comparative study with chronic hepatitis B. *Gastroenterology.* **104**:595–603.
42. Moriya, K., et al. 2001. Increase in the concentration of carbon 18 monounsaturated fatty acids in the liver with hepatitis C: analysis in transgenic mice and humans. *Biochem. Biophys. Res. Commun.* **281**:1207–1212.
43. Barbaro, G., et al. 1999. Hepatocellular mitochondrial alterations in patients with chronic hepatitis C: ultrastructural and biochemical findings. *Am. J. Gastroenterol.* **94**:2198–2205.
44. Hui, J.M., et al. 2003. Insulin resistance is associated with chronic hepatitis C virus infection and fibrosis progression [corrected]. *Gastroenterology.* **125**:1695–1704.
45. Kato, J., et al. 2001. Normalization of elevated hepatic 8-hydroxy-2′-deoxyguanosine levels in chronic hepatitis C patients by phlebotomy and low iron diet. *Cancer Res.* **61**:8697–8702.
46. Horiike, S., et al. 2005. Accumulation of 8-nitroguanine in the liver of patients with chronic hepatitis C. *J. Hepatol.* **43**:403–410.
47. Takenaka, K., et al. 1994. Possible multicentric occurrence of hepatocellular carcinoma: a clinicopathological study. *Hepatology.* **19**:889–894.
48. Oikawa, T., et al. 2005. Multistep and multicentric development of hepatocellular carcinoma: histological analysis of 980 resected nodules. *J. Hepatol.* **42**:225–229.
49. Akiyama, T.E., et al. 2001. Peroxisome proliferator-activated receptor-α regulates lipid homeostasis, but is not associated with obesity. *J. Biol. Chem.* **276**:39088–39093.
50. Nakajima, T., et al. 2004. Peroxisome proliferator-activated receptor α protects against alcohol-induced liver damage. *Hepatology.* **40**:972–980.
51. Ni, R., et al. 1994. Fas-mediated apoptosis in primary cultured mouse hepatocytes. *Exp. Cell Res.* **215**:332–337.
52. Graulet, B., Gruffat, D., Durand, D., and Bauchart, D. 1998. Fatty acid metabolism and very low density lipoprotein secretion in liver slices from rats and preruminant calves. *J. Biochem.* **124**:1212–1219.
53. Folch, J., Lees, M., and Sloane Stanley, G.H. 1957. A simple method for the isolation and purification of total lipids from animal tissues. *J. Biol. Chem.* **226**:497–509.
54. Gurtu, V., Kain, S.R., and Zhang, G. 1997. Fluorometric and colorimetric detection of caspase activity associated with apoptosis. *Anal. Biochem.* **251**:98–102.

ELSEVIER

Journal of Hepatology 48 (2008) 858–879

Journal of Hepatology

www.elsevier.com/locate/jhep

Review

Experimental models of hepatocellular carcinoma☆

Philippa Newell[1,2], Augusto Villanueva[1], Scott L. Friedman[1], Kazuhiko Koike[3], Josep M. Llovet[1,4,*]

[1]*Division of Liver Diseases, Mount Sinai School of Medicine, 1425 Madison Avenue, Box 1123, New York, NY 10029, USA*
[2]*Department of Surgery, Mount Sinai School of Medicine, 1425 Madison Avenue, Box 1123, New York, NY 10029, USA*
[3]*Department of Infectious Diseases, Internal Medicine, Graduate School of Medicine, University of Tokyo, Japan*
[4]*BCLC Group, Liver Unit, IDIBAPS, CIBERehd, Hospital Clinic, Barcelona, Spain*

Hepatocellular carcinoma (HCC) is a common and deadly cancer whose pathogenesis is incompletely understood. Comparative genomic studies from human HCC samples have classified HCCs into different molecular subgroups; yet, the unifying feature of this tumor is its propensity to arise upon a background of inflammation and fibrosis. This review seeks to analyze the available experimental models in HCC research and to correlate data from human populations with them in order to consolidate our efforts to date, as it is increasingly clear that different models will be required to mimic different subclasses of the neoplasm. These models will be instrumental in the evaluation of compounds targeting specific molecular pathways in future preclinical studies.

Keywords: **Liver cancer; Hepatocellular carcinoma; Mouse models; Genetically engineered mice; Cirrhosis**

1. Introduction

Hepatocellular carcinoma is one of the world's deadliest cancers, ranking third among all cancer-related mortalities. Most cases occur in Asia and sub-Saharan Africa, where viral hepatitis is endemic. The incidence is rising in the West, likely due to the increase in patients infected with hepatitis C during the latter half of the last century [1]. The liver, unique in its capacity for regeneration following injury, also gives rise to this malignancy commonly associated with the inflammatory state of advanced fibrosis, or cirrhosis. Potentially curative therapies can be offered to approximately 30% of patients, but are complicated by a high rate of recurrence [2].

Encouraging progress has been made in understanding the molecular pathogenesis of cancer [1,2]. The discoveries of the signal transduction pathways, cascades of protein–protein interactions transmitting information from the cell surface to the nucleus, and of their link to tumor biology, are particularly impressive.

Several key mouse models have been instrumental in defining the pathogenesis of HCC by introducing genetic

Associate Editor: M. Colombo

☆ P. Newell is a recipient of an American Liver Foundation (ALF) Postdoctoral Research Fellowship Award (2007). A. Villanueva is supported by grants from the Fundacion Caixa Galicia and the National Cancer Center. S. Friedman is a Professor of Medicine and Chief of the Division of Liver Diseases, supported by NIH Grant number DK37340. K. Koike is Chairman of Department of Infectious Diseases, University of Tokyo, supported by grant from the Ministry of Health, Labor and Welfare, and Ministry of Education, Science, Sports and Culture of Japan. J.M. Llovet is Director of the HCC Program in Mount Sinai and Professor of Research-ICREA in the Hospital Clínic Barcelona, supported by National Institute of Health-NIDDK grant 1R01DK076986-01, National Institute of Health-I+D Program (Spain) grant number SAF-2007-61898. The authors declare that they do not have anything to disclose regarding funding from industries or conflict of interest with respect to this manuscript.

* Corresponding author. Address: Division of Liver Diseases, Mount Sinai School of Medicine, 1425 Madison Avenue, Box 1123, New York, NY 10029, USA. Tel.: +1 212 659 9503; fax: +1 212 849 2574.
E-mail address: josep.llovet@mssm.edu (J.M. Llovet).

Abbreviations: HCC, hepatocellular carcinoma; HCV, hepatitis C virus; TKR, tyrosine kinase receptor; HBV, hepatitis B virus; TSG, tumor suppressor gene; TSP, tissue specific promoter; Tg, transgene.

0168-8278/$32.00
doi:10.1016/j.jhep.2008.01.008

alterations into one or more aetiologic pathways that can be targeted exclusively to the liver. Moreover, these programmed manipulations can be introduced systematically, not only in this specific organ but also at defined times during development, growth and aging of the liver.

Nonetheless, substantial challenges persist in modeling liver diseases whose natural history requires a chronic inflammatory milieu. For example, infectious (hepatitis C virus), toxic (alcohol), metabolic (non-alcoholic steatohepatitis), or congenital (hemachromatosis) diseases share inflammation and fibrosis as precursors to cancer, yet none is easily mimicked in animals. There are few rodent models of HCC arising spontaneously within a background of regenerative nodules and cirrhosis, and most depend on the administration of hepatotoxic and/or carcinogenic agents to recreate the injury–fibrosis–malignancy cycle seen in chronic human liver diseases.

Comparative genomic studies in human HCC samples have begun to identify molecular subgroups with characteristic mutations, gene expression profiles and chromosomal gains and losses [3]. Moreover, since there is no single dominant molecular pathology underlying all HCCs, it is increasingly clear that different models will be required to mimic different subclasses of the neoplasm. These models will be instrumental as pre-clinical tools to evaluate compounds targeting specific molecular pathways.

With these challenges in mind, the objective of this review is to assemble and evaluate the available models of both cirrhosis and HCC, to provide a blueprint for understanding the pathogenesis of HCC and for optimizing preclinical models for drug testing.

2. Experimental models in cancer research

Although many experiments focusing on liver physiology have been conducted in rats due to their propensity for the development of fibrosis, the laboratory mouse (*Mus musculus*) is considered among the best model systems for cancer because of the availability of gene targeting methods, as well as the animal's size and breeding capacity, its lifespan of 3 years, and its physiologic and molecular similarities to human biology [4]. Significant advances have been made in modeling cancer genetics in mice, along a spectrum that ranges from simple xenograft models to more complex, genetically modified mice. Examples of each of the following are illustrated in Table 1.

2.1. Xenograft models

The demonstration that concentrated cancer cells grown *in vitro* could form tumors when implanted subcutaneously into an immunocompromised mouse was first established in 1969 [5]. This xenograft model has since demonstrated several advantages that explain its persistence as the mainstay of pre-clinical studies of anti-neoplastic drugs *in vivo*: the tumors are rapidly and easily induced, and their subcutaneous location enables direct measurement of tumor growth. More recently, however, several critical differences between xenograft- and patient-derived specimens have become apparent, as discussed below. In addition, cancer is now appreciated as a complex disease dependent upon the interaction between transformed cells harboring oncogenic mutations, referred to as the 'cell autonomous compartment', and their surrounding tumor environment, the 'non-cell autonomous constituents' made up of normal cells, stromal cells, and immune cells [4], features that are not part of the xenograft approach.

Mouse models of cancer were first introduced over 60 years ago. Shortly after its inception in 1955, the Developmental Therapeutics Program at the National Cancer Institute (NCI) adopted the use of three transplanted rodent models of sarcoma, carcinoma, and leukemia, for the purposes of selecting agents for clinical use in cancer patients. Thousands of molecules were tested in mice bearing murine leukemias during the first decades of modern cancer drug development, circa 1945–1969 [6]. This tumor panel was later expanded to include human tumor xenografts, with the intention to study drug activity against solid tumors [7]. In 1990, the NCI focused on the development of *in vitro* assays in 60 different cell lines in order to screen pharmaceutical agents for their potency and their selective activity against either a particular disease category or specific cell line [8,9], the most promising of which were to be subsequently evaluated in the nude mouse xenograft model.

The validity of xenografts as a predictive indicator of probable clinical activity is limited, with the most success seen in cytotoxic agents. A retrospective analysis performed by the NCI for 39 compounds in which both xenograft testing and Phase II clinical data were available showing that less than 50% of agents with activity in more than one-third of xenografts showed clinical activity ($p = 0.04$) [6]. The same study demonstrated that activity in a particular histology in a tumor model did not closely correlate with activity in the same human cancer histology [10], with the exception of non-small cell lung and ovarian cancer [11].

There are several variables inherent to the xenograft experiments which may impact on the divergent outcomes compared to human disease, including growth properties and size at initiation of treatment of xenograft tumor, ectopic versus orthotopic location of tumor, local versus metastatic disease [12], tolerance for high doses of chemotherapeutic agents in mice [13],

Table 1
Available mouse models in cancer research

	Technical Method	Advanced Mouse Models of Cancer	Current Models in HCC	Future Prospects: Wish List for HCC
Xenograft	Xenograft 	COLON, BREAST, PROSTATE: Surgical orthotopic implantation: intact fragments of human cancer, including tumors taken directly from the patient, transplanted into the corresponding organ of immunodeficient rodents[16]	Orthotopic xenograft model in which hepatoma 129 cells originating from C3H mice are injected into fibrotic livers of mice pretreated with TAA and EtOH[45]	Mouse HCC cell line derived from GEM tumor with specific molecular pathway dysregulated, with immunofluorescent marker, injected into fibrotic liver of immune-competent mice
Transgenic GEM	Constitutive Transgenic 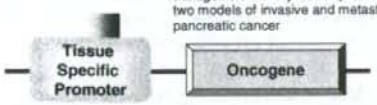	PANCREATIC: $Kras^{G12V}$ and chronic pancreatitis[169]; $Trp53^{R172H}$ and $Kras^{G12D}$ double transgenic driven by insulin promoter[170]; two models of invasive and metastatic pancreatic cancer	Mouse C-myc/Human E2F-1 overexpression driven by albumin promoter[171]; HCC at 6-8 months	Double transgenic overexpressing profibrotic gene combined with liver-specific oncogene
	Dominant Negative Transgenic 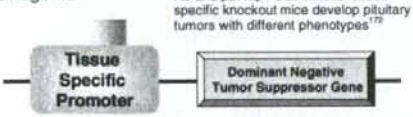	PITUITARY: Rb and p27Kip1 Cdk inhibitor tissue specific knockout mice develop pituitary tumors with different phenotypes[172]	Mdr-2 knockout mice are unable to secrete phospholipids into bile, and develop cholangitis and HCC at 6-12 months[166]	Double transgenic liver-specific E-cadherin knockout and β-catenin overexpression
	Inducible Transgenic 	MELANOMA: Double transgenic combining Tet-induced overexpression of mutated $Hras^{Y12D}$ and Ink4a knockout[173]	Tet-inducible Met expression under albumin promoter: 60% HCC at 12 months; tumors regressed when transgene (Tg) was inactivated[91]	Tet-induced, liver-specific overexpression of known oncogene in fibrotic mice
Endogenous GEM	Conditional Gene Targeting 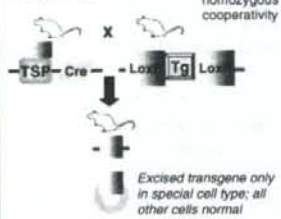	PROSTATE: Double transgenic Cre-mediated $PTEN^{-/-}$ homozygous loss and $p19Arf^{-/-}$: cooperativity in cancer development[174]	Cre-mediated liver specific PTEN-/- knockout: 66% HCC at 8 months[108]	Cre-mediated, liver-specific knockout of known tumor suppressor gene in fibrotic mice

and variability in selected endpoints. These variables can be minimized if given due consideration in the design of preclinical cancer drug experiments. However, the greatest discrepancies between success of cancer therapies in xenograft models and in human clinical trials are likely due to critical differences in both the tumor cells and their microenvironment. Natural tumor progression is a micro-evolutionary process during which increasingly aggressive clones, generated through genetic instability, emerge from an initially monoclonal lesion. Autochthonous tumors, those that evolve *in situ* from normal cells, tend to have a diminished genetic heterogeneity compared to tumor xenografts, although selective pressures of cell culture or tissue explantation can cause a rapid expansion of a certain clonal constituent of polyclonal tumors [14,15].